Microstructure and Texture Development in AZ31 Magnesium Alloy Processed by Equal Channel Angular Pressing

by

Linda Vuong

Department of Mining, Metals and Materials Engineering
McGill University
Montreal, Canada

July 2006

A thesis submitted to the Faculty of Graduate and Postdoctoral Studies in fulfillment of the requirements of the degree of Master of Engineering

Your file Votre référence
ISBN: 978-0-494-28631-9
Our file Notre référence
ISBN: 978-0-494-28631-9

ABSTRACT

Enhancement of the ductility is very important for the successful commercialization of magnesium alloys. Among other methods, this can be achieved by refining the grain structure through equal channel angular pressing (ECAP) or extrusion. Preliminary work was conducted using as-cast AZ-31, but this was found to be of low ductility and extruded bars were used for the rest of the experimentation. These were annealed at 350°C for 1 hour and extrusion was carried out at three temperatures, 200, 250 and 300°C, using routes A, B_C and C at a speed of 5 mm/s for up to 8 passes. It is apparent that increasing the operating temperature increases the final grain size as a result of grain growth. Conversely increasing the number of passes results in a finer grain size because of the accumulation of shear. However, grain growth can affect the final grain size for all three routes. After one ECAP pass, a preferred orientation with the basal planes inclined at 45° to the ECAP axis is observed. For route A, as more and more passes are employed, the original fiber texture tends towards a rolling texture. By contrast, for route C, repeating the ECAP steps does not change the texture, which retains the 45° preferential orientation. The mechanical properties indicate that using a path with shearing in more directions, such as route C, results in increased ductility, with a wider flow curve than for route A. As the temperature of ECAPping is increased, the strength of the extruded product increases and the ductility decreases. This appears to be due to the coarser grain size of the 300°C product and indicates that the effect of grain refinement is greater than that of texture.

RÉSUMÉ

Un aspect important pour la réussite de la commercialisation des alliages de magnésium est l'amélioration de leur ductilité. Plusieurs méthodes peuvent être utilisées afin d'atteindre ce but. L'extrusion angulaire à section constante (*equal channel angular pressing* – ECAP) constitue une possibilité. Une étude préliminaire a été menée sur l'alliage AZ 31 brut de coulée, mais cet alliage s'est avéré trop fragile et des barreaux extrudés ont été utilisés pour les essais ultérieurs. Ces barreaux ont subi un recuit à 350°C pendant une heure et les extrusions ont été réalisées à trois températures différentes (200, 250 et 300°C) en utilisant les voies A, B_C et C à une vitesse de 5mm/s. Les échantillons ont été déformés jusqu'à 8 passes. Il a été démontré que l'augmentation de température mène à un grossissement de la microstructure finale, qui est attribuable principalement à la croissance des grains. De plus, une augmentation du nombre de passes provoque une diminution des tailles de grains à cause d'une accumulation du cisaillement. Cependant, les trois voies de production peuvent être affectées par un grossissement de la taille des grains. Après une passe d'ECAP, on observe une orientation préférentielle des grains, avec les plans basaux inclinés à 45° par rapport à la direction d'extrusion. Pour la voie A, lorsque le nombre de passes augmente, la texture originale de fibre se transforme en une texture de laminage. La voie C, au contraire, ne change pas la texture et l'inclinaison de 45° est conservée. Les propriétés mécaniques indiquent que les voies qui provoquent du cisaillement dans des plans différents, telle la voie C, augmentent la ductilité comparativement à la voie A. La résistance mécanique des produits extrudés augmente avec la température, tandis que la ductilité diminue. Ceci paraît être dû à la taille de grain plus importante des produits extrudés à 300°C et ceci indique donc que les effets liés au raffinement des grains sont plus importants que ceux liés à la texture.

ACKNOWLEDGEMENTS

Firstly, I would like to thank my mentor and supervisor, Professor John J. Jonas, at McGill University. His great knowledge as well as his love of and dedication to his work and his students inspired me greatly. As well, I am grateful to Stéphane Godet for his support, guidance and incredible help.

Secondly, many thanks go out to the staff and students at McGill University's Department of Mining, Metals and Materials Engineering: Lan Jiang for her patience and imparting her great knowledge of magnesium alloys to me as well as her help in the analysis of results and Rocco Varano for his help and guidance during sample preparation. I would also like to thank Edwin Fernandez for all of his work and machining.

Lastly, I would like to take the time to thank some sponsors from the Catholic University of Leuven and from General Motors. Professors B. Verlinden and P. Van Houtte, and Drs. Joke De Messemaeker and Miljana Popovic of the Department of Metallurgy and Materials Engineering (MTM), Faculty of Engineering, Catholic University of Leuven (KULeuven), Heverlee, Belgium were incredibly helpful in giving advice during experimentation on their ECAP machine. I also want to acknowledge Drs. Alan Luo and Anil Sachdev, first for giving me the immense opportunity of interning with them at the General Motors Technology Center, but also for their input throughout my master's project.

And of course, my mother, my sister and my friends and colleagues, who have supported me for these and other years.

TABLE OF CONTENTS

LIST OF FIGURES

CHAPTER 5

LIST OF TABLES

CHAPTER 2

CHAPTER 5

CHAPTER 1 - INTRODUCTION

While magnesium is known to be the lightest structural metal in common use, there is an important disadvantage to using this metal. This is closely related to its hexagonal crystal structure, which significantly lowers its room temperature ductility. While alloying improves its properties and allows it to be used in engineering applications, there is still considerable room for improvements to be made [1].

The major alloys used in industry are from the magnesium-aluminum-zinc family because of their optimal combination of light weight and strength. Nonetheless it remains difficult to deform these alloys plastically because the HCP structure renders dislocation motion in the crystal lattice difficult at ambient temperature restricting most of the uses of magnesium alloys to castings and hot formed parts.

For automotive applications, it is critical to have good ductility when parts are being formed. Ductility enhancement is therefore one of the most important goals associated with the increased use of magnesium alloys in this industry. It has been demonstrated that the ductility can be improved by grain refinement in such alloys.

By contrast, a strong alignment of the basal planes takes place during the extension of magnesium alloys. This makes subsequent deformation more difficult than when the texture is random.

1.1. Objective

Equal channel angular pressing (ECAP) is a procedure whereby severe plastic deformations [2] can be produced in a variety of materials without significantly changing the geometric shapes of the samples. During the process of ECAP, a billet experiences simple shear without any cross-sectional area change, as shown in Figure 1.1. It can be used to produce ultra-fine grain sizes in the submicrometer or nanometer range by introducing large plastic strains. It has been proven to be effective in enhancing the mechanical properties at room temperature and in leading to superplasticity at elevated temperatures in aluminum alloys. In magnesium alloys, low temperature superplasticity can be produced by processing with ECAP.

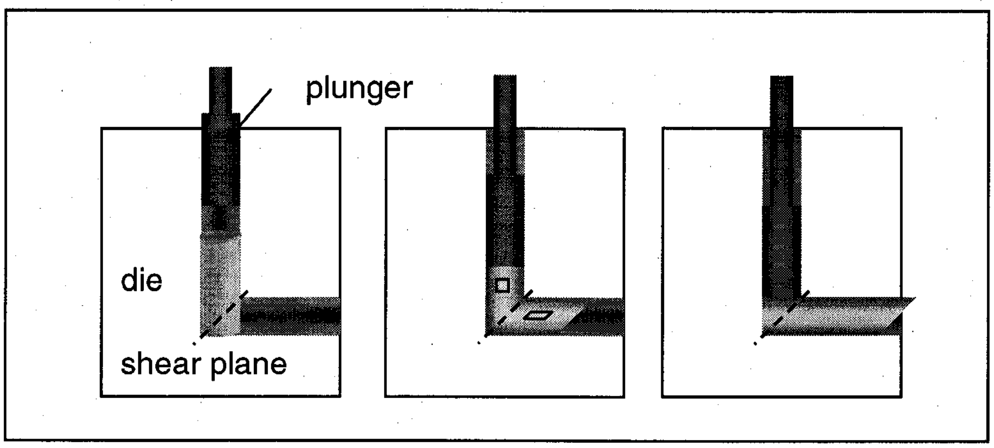

Figure 1.1. Schematic of the ECAP process.

The objective of this work was to study the effect of ECAP on magnesium-Al3%-Zn1% (AZ31) alloy in terms of the microstructures produced along diverse routes by deformation at different temperatures. This was done with the aim of expanding the understanding of the deformation mechanisms and characteristics of AZ31 in terms of texture development and microstructure evolution during severe plastic deformation. While a similar process is not applicable to industry, it is imperative to improve present processing methods by providing insight into methods for the improvement of the mechanical properties of magnesium alloys by deformation processing. ECAP has been known to be a method for producing grain refinement and therefore the observation of its effect could prove to be very useful [3].

1.2. Thesis Outline

The thesis consists of 6 chapters:

Chapter 2 is a literature review in which past work related to deformation mechanisms of magnesium and its alloys are surveyed. Then work more specifically pertaining to equal channel angular extrusion together with the microstructure and texture evolution produced using this method is reviewed. Finally, applications of ECAP including superplasticity are covered.

In Chapter 3, experimental details are provided regarding materials and equipment as well as methods of analysis.

The evolution of the microstructure and texture in the magnesium samples extruded using ECAP is described in Chapter 4, as well as the subsequent mechanical properties determined by compression testing.

The results presented in the previous chapter are then thoroughly discussed in Chapter 5 in terms of microstructure and texture development and the effect on the final mechanical properties as well as the realities facing the magnesium alloy industry.

The final chapter includes a few concise conclusions about the findings of the project.

CHAPTER 2 - LITERATURE REVIEW

2.1. Magnesium and Magnesium Alloys

Metallic magnesium, with a density of $1.74 g/cm^3$, is the lightest of all commonly used structural metals [1]. However, since the strength of pure magnesium at room temperature (about 90 MPa) is insufficient for most structural uses; it is usually alloyed with other metals to increase its strength. For engineering applications, magnesium is alloyed mainly with aluminum, zinc, manganese, rare earth metals and zirconium to produce alloys with high strength-to-weight ratios. They are then attractive for such applications as automotive, railway and aerospace parts [4].

The resulting alloys, however, remain difficult to deform plastically at room temperature because of the hexagonal closed packed (HCP) crystal structure of elemental magnesium. This restricts slip to the basal planes leading to low ductility at room temperature. Higher temperatures allow other slip systems to be activated and so magnesium alloys need to be worked at temperatures above ambient. For this reason, magnesium alloys for engineering designs are usually employed in the form of castings as opposed to the wrought form due to the difficulty of cold working [4].

Magnesium-aluminum-zinc casting alloys are of major industrial importance because of their combination of light weight, strength, and relatively good corrosion resistance. The addition of zinc to Mg-Al alloys increases strength by both solid solution and precipitation hardening [5].

The evolution of flow stress in magnesium alloys is sensitive to texture and deformation mode, leading to a large variation in flow stress. This is accounted for by the limited slip systems available in the magnesium lattice and the influence that prismatic slip, twinning and dynamic recrystallization have on the flow stress and structure [5].

2.1.1. *Classification and Nomenclature of Magnesium Alloys*

Magnesium alloys are usually designated by two capital letters followed by two numbers. The letters indicate the main alloying elements in decreasing order of concentration. The numbers that follow respectively indicate the weight percent of each element. If a letter follows the numbers, A, B, etc., there has been a slight modification to the alloy in the form of the impurity levels. The codes for alloying elements are displayed in Table 2.1. E.g. AZ91 designates a magnesium alloy containing 9 wt.% aluminum and 1 wt.% zinc.

Table 2.1. Alloying elements employed in magnesium alloys and the letters used in the nomenclature.

Alloying Element	**Code Letter**
Aluminum	A
Zinc	Z
Manganese	M
Rare Earths	E
Thorium	H
Zirconium	K
Silver	Q
Tin	T
Yttrium	W
Silicon	S

2.1.2. *Deformation: Hexagonal Closed Packed Slip Systems*

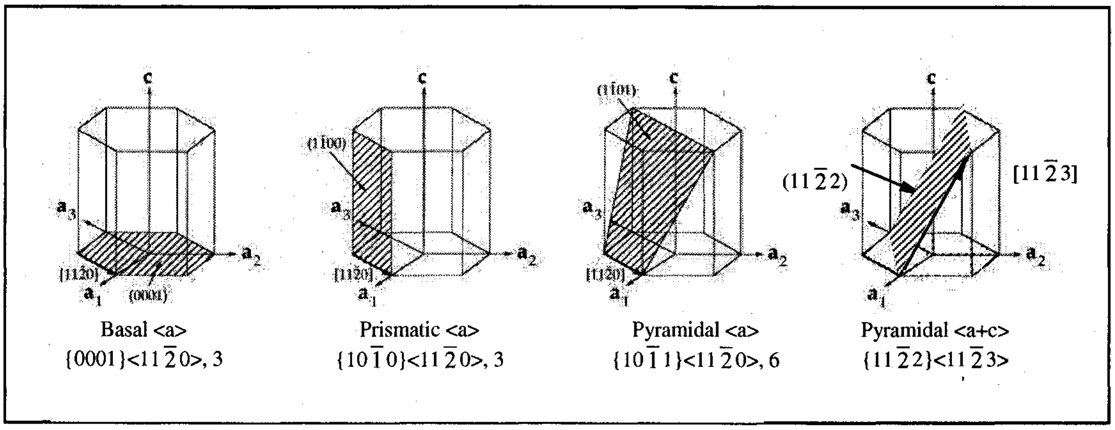

Figure 2.1. Basal, prismatic and pyramidal slip systems in hcp materials.

The dominant intragranular deformation mechanisms are i) slip on the basal $\{0001\}\langle 11\bar{2}0\rangle$, prismatic $\{10\bar{1}0\}\langle 11\bar{2}0\rangle$ and pyramidal $\{10\bar{1}1\}\langle 11\bar{2}0\rangle$ systems, and ii) twinning on the pyramidal $\{10\bar{1}2\}\langle \bar{1}011\rangle$ plane, all shown in Figure 2.1. The strain hardening of polycrystals has been attributed primarily to crystal lattice reorientation during deformation. The most important mechanism of rapid crystal lattice reorientation is mechanical twinning [6].

The easy slip directions $\langle 11\bar{2}0\rangle$ are perpendicular to the c-axis. In order to accommodate straining along the c axis, slip or twinning along the <c+a> slip/twin direction must be activated. At low temperatures, deformation twinning is the dominant available mechanism, which allows for inelastic shape changes in the c-direction. At high temperatures, slip along the $\langle 11\bar{2}0\rangle$ and $\langle 11\bar{2}3\rangle$ directions becomes possible and the slip planes containing these directions are the first-order $\{10\bar{1}1\}$ and second-order $\{11\bar{2}2\}$ pyramidal planes [6].

The deformation of HCP materials at room temperature typically occurs as a result of crystallographic slip and deformation twinning occurring simultaneously; the resulting mechanical properties are then strongly affected by the interaction between these two major mechanisms of inelastic deformation. Magnesium and its alloys deform essentially by basal slip and twinning, which limits their formability [7]. In extruded rods of HCP materials, the basal planes of the grains will be strongly aligned parallel to the longitudinal axis of the rod. Consequently, a compressive strain induced parallel to the basal poles favours contraction twinning, while a tensile strain in the same direction produces extension twins [8].

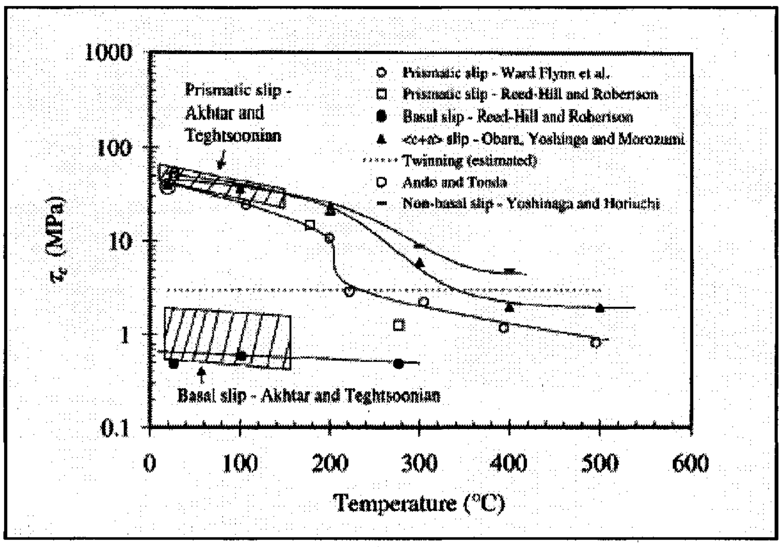

Figure 2.2. Critical resolved shear stress vs. temperature for magnesium alloys.

The critical resolved shear stress (CRSS) for basal plane slip in magnesium single crystals exhibits a 100 times lower value than that of non-basal plane slip near room temperature, as seen in Figure 2.2. The amount of basal slip plays an important role in the enhancement of mechanical properties at room temperature. Nevertheless, the full accommodation of plastic deformation at room temperature requires dislocation slip on other glide planes or extensive contributions from twinning.

2.1.3. Deformation Twinning

While twins act as barrier to dislocation movement, they reorient basal planes to accommodate deformation. For magnesium alloys, three types of twins are known: extension twins, contraction twins and double twins [9]-[12]. Only extension twins allow for extension along the c-axis of the crystallographic texture component, while contraction twins accommodate compression along the c-axis. For this reason, extension twinning is preferred when there is an extension strain component parallel to the c-axis or when contraction is being applied perpendicular to the c-axis. In addition, extension twinning has a low CRSS of 2-4 MPa and is therefore easily activated [13].

Contraction twinning will be activated when the contraction strain is parallel to the c-axis or when extension is perpendicular to the c-axis. On the other hand, contraction twinning has a high CRSS of 76-153 MPa, making it very difficult to activate [13].

Because of the difference between extension twins and contraction twins referred to above, the stress-strain curves in tension and compression obtained on extruded magnesium samples are very different. Extension twinning has a very low critical resolved shear stress (2-4 MPa), while contraction twinning has a high CRSS (76-153 MPa). Furthermore, the reorientations produced by these types of twins are also very different: 86° for $\{10\bar{1}2\}$ extension twins and 56° for $\{10\bar{1}1\}$ contraction twins (Figure 2.3). In compression, yielding occurs at a stress level that is almost half of that in tension. This tension-compression asymmetry makes magnesium and its alloys a good option for structural materials since they will deform in compression (during forming) before tension (during loading) [13].

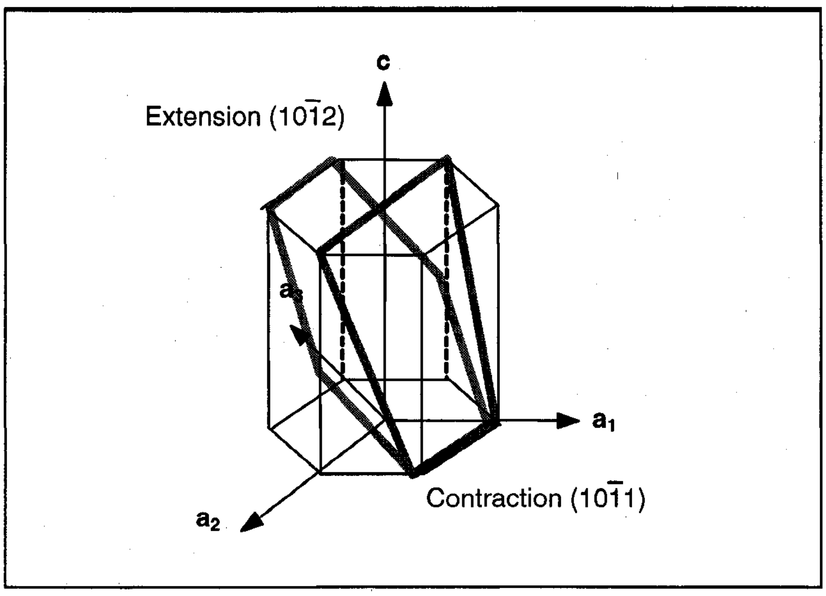

Figure 2.3. Twinning systems in hcp materials [13].

Once primary twinning has taken place, secondary twinning can occur within the reoriented primary twins. This is known as double-twinning, shown in Figure 2.4. Contraction twinning has the effect of rotating the basal planes towards a more favourable orientation for slip. Double twinning has the same effect. Extension twinning reorients the basal planes by 86° [13].

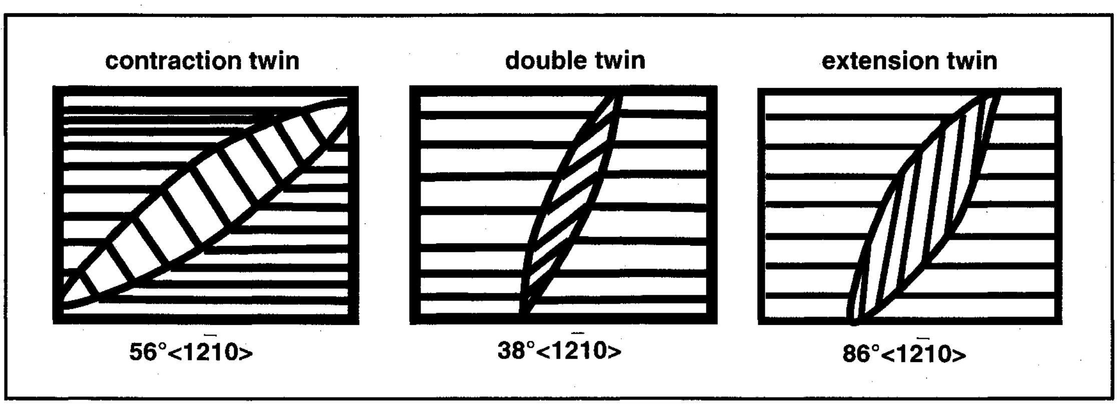

Figure 2.4. Diagram of slip plane rotations within twins [13].

2.1.4. *Deformation Textures*

A. Fiber (Extrusion) Textures

This texture is defined by the basal planes being aligned to be perpendicular to the extrusion axis in a cylindrical texture. This texture is usually found in axisymmetrically extruded rods [14].

B. Rolling Textures

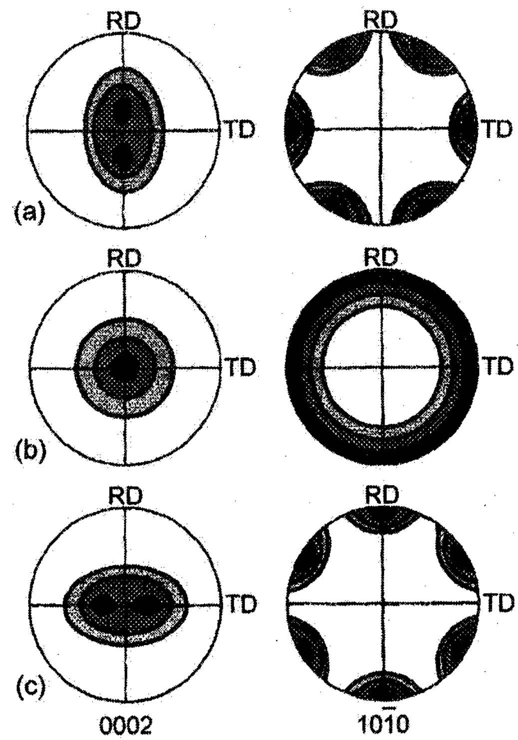

Figure 2.5. Schematic of (0002) and ($10\bar{1}0$) pole figures for rolling textures in HCP metals with c/a ratios of (a) greater than 1.633, (b) approximately equal to 1.633 and (c) less than 1.633 [14].

Mg – 1.624

The textures found in cold rolled HCP metals are categorized according to their c/a ratios, as illustrated in Figure 2.5. Metals with c/a ratios greater than the ideal value (1.633) exhibit textures with basal poles tilted at 15 to 25° away from the normal direction toward the rolling direction and [$11\bar{2}0$] poles aligned with the rolling direction. Magnesium, however, has a c/a ratio very close to ideal and therefore tends to form [0001] fiber textures. By contrast, metals, with c/a ratios below ideal tend to form textures with the basal poles tilted 20 to 40° away from the normal direction toward the transverse direction and the $[10\bar{1}0]$ poles aligned with the rolling direction. Other factors such as strain rate, temperature and chemical composition also influence texture development [14].

C. Tube Textures – Zirconium

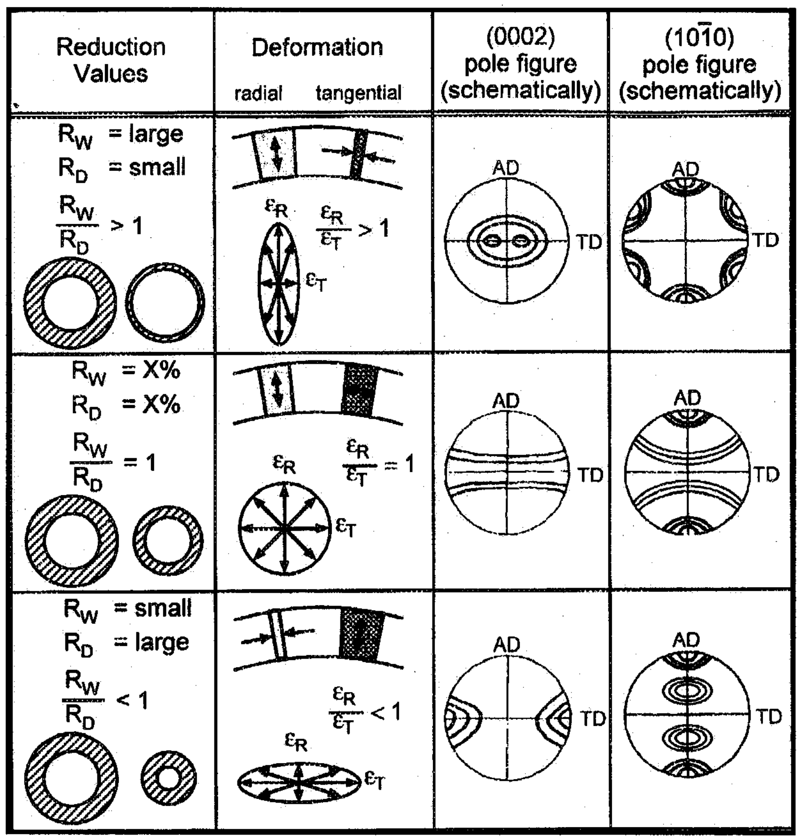

Figure 2.6. Schematic summarizing tube textures for zircaloy for various reduction values. ε_R is the radial strain and ε_T is the tangential (or hoop) strain [14].

A considerable amount of texture analysis of zirconium and zirconium alloys has focused on tube materials because of their use in the cladding of nuclear reactor fuels. A schematic summary of these results is shown in Figure 2.6. The textures in this summary are given on the assumption of a random initial texture and are for extreme reductions. It should also be noted that the texture expected for $R_W/R_D = 1$ is similar to that expected for wire drawing and the texture expected for $R_W/R_D > 1$ is similar to that expected for rolled sheet (where R_W: reduction in wall thickness; R_D: reduction in diameter).

2.2. Equal Channel Angular Pressing or Extrusion (ECAP or ECAE)

2.2.1. Ductility Enhancement

To be useful for automobile components, a material should exhibit good ductility as well as strength, since components often fracture by ductile processes. Magnesium alloys generally fail in a brittle mode with a low elongation to failure of less than 10% due to its HCP crystal structure. For magnesium to be usable for components, it is therefore necessary to enhance its ductility [4].

It has been demonstrated that the ductility of WE43 magnesium alloy can be enhanced by grain refinement by deformation at a strain rate of about 2×10^{-3} s^{-1}. The enhancement of the ductility is then due to a transition in the fracture behaviour as a result of refining the microstructure. Refining the microstructure makes it possible to develop a structural magnesium alloy with high ductility [15].

Extruded AZ80 magnesium alloy exhibits a strong texture, whereby the majority of the basal planes are arranged parallel to the extrusion direction. Subsequent deformation perpendicular to the extrusion direction is therefore limited and the alloy fractures without macroscopic necking. To enhance the ductility, it is possible to refine the grain structure and to modify the texture by rearranging the distribution of basal planes in the wrought magnesium. A way of doing this is ECAP [3], [16]-[21].

2.2.2. ECAP

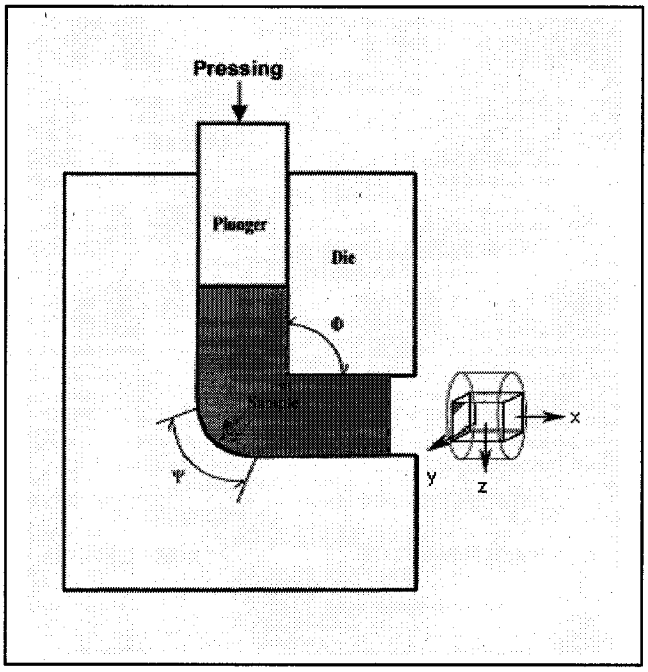

Figure 2.7. Schematic of an ECAP die [22].

ECAP is a unique technique for applying heavy shear strains to a material in order to develop ultra-fine grained structures by recrystallization. These can be in the submicrometer or nanometer range for a variety of metals and alloys. During the process of ECAP, a billet experiences simple shear without any cross-sectional area change (Figure 2.7). This is achieved by pressing a sample, cylindrical or rectangular, through a die in which two channels of equal cross-section intersect at an angle Φ. An additional angle Ψ defines the arc of curvature at the outer point of intersection of the two channels, as seen in Figure 2.5. The strain, ε, induced is given by:

$$\varepsilon = \left(\frac{2\cot\left(\frac{\Phi}{2}+\frac{\Psi}{2}\right) + \Psi \operatorname{cosec}\left(\frac{\Phi}{2}+\frac{\Psi}{2}\right)}{\sqrt{3}} \right) \tag{1}$$

where Ψ is in radians.

The sample can be run through this die many times, achieving severe plastic deformations; the total strain can then be determined from:

$$\varepsilon_{tot} = N\varepsilon \qquad (2)$$

where N is the number of passes [23].

Nakashima *et al.* have shown that the development of ultra-fine grain structures, with equiaxed grains separated by high angle boundaries, is achieved by imposing intense plastic strains in a single pass, a process that is most effective with a $\Phi = 90°$ die [21]. After one pressing through an ECAP 90° die, a cubic element is sheared into a rhombohedral shape, as seen in Figure 2.8.

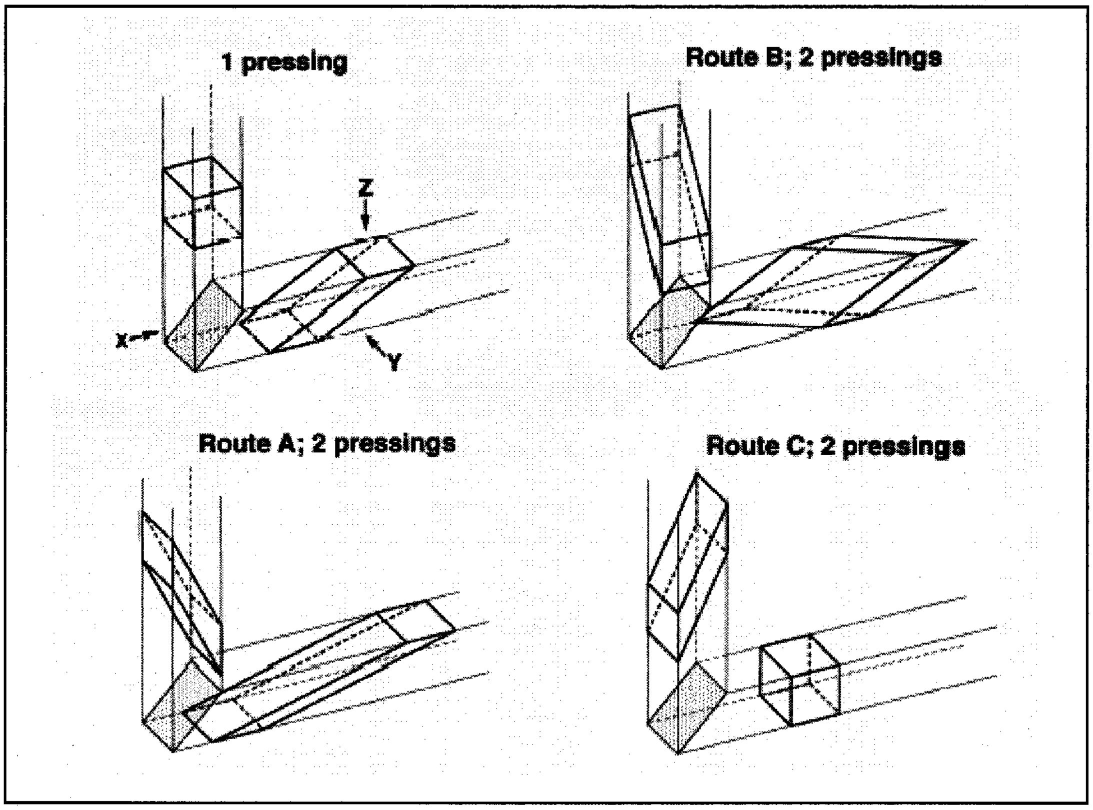

Figure 2.8. Schematic illustration of shearing planes following given routes. X, Y, Z define three orthogonal planes of observation [24].

However, the shape of the cube determined by subsequent pressings will depend on the rotation of the sample before it re-enters the die. There is an infinite number of processing routes that can be followed with this method using all possible angles of rotation. But six simple routes have been defined, as seen in Table 2.2 [24].

Table 2.2. Rotation angles and directions at each pressing defining six possible routes [24].

Route	Number of pressings						
	2	3	4	5	6	7	8
A	0°	0°	0°	0°	0°	0°	0°
B_A	90° ↖	90° ↘	90° ↖	90° ↘	90° ↖	90° ↘	90° ↖
B_C	90° ↖	90° ↖	90° ↖	90° ↖	90° ↖	90° ↖	90° ↖
C	180°	180°	180°	180°	180°	180°	180°
B_A-A	90° ↖	0°	90° ↘	0°	90° ↖	0°	90° ↘
B_C-A	90° ↖	0°	90° ↖	0°	90° ↖	0°	90° ↖

Using these definitions, it is possible to observe the effect of consecutive passes for each route on the shearing planes x, y and z. It is possible to conclude that routes B_C and C are preferable to routes B_A and A because of the restoration of the shape of the cubic element produced by the former routes, as seen in Table 2.3. In addition, route B_C would appear to be favourable due to the absence of deformation in the z-plane in route C. Combining elements of routes can also create more suitable routes. However, route B_A-A simply increases distortion with further pressing in the three orthogonal planes while route B_C-A represents optimum pressing conditions because it introduces high shear strains in each plane and still restores the cubic element after a total of 8 pressings.

The information in the following table can be used to predict the dominant characteristics of texture development. For example a strong rolling texture can be produced using route A while an extrusion texture would be found in samples processed by route B_A. By contrast, routes B_C and C can be expected to develop only limited textures [24]. Route B_C has been reported to be the most effective for grain refinement resulting in a larger increase in the room temperature ductility of AZ alloys [16], [25]-[27].

Table 2.3. Shearing characteristics for six different processing routes [24].

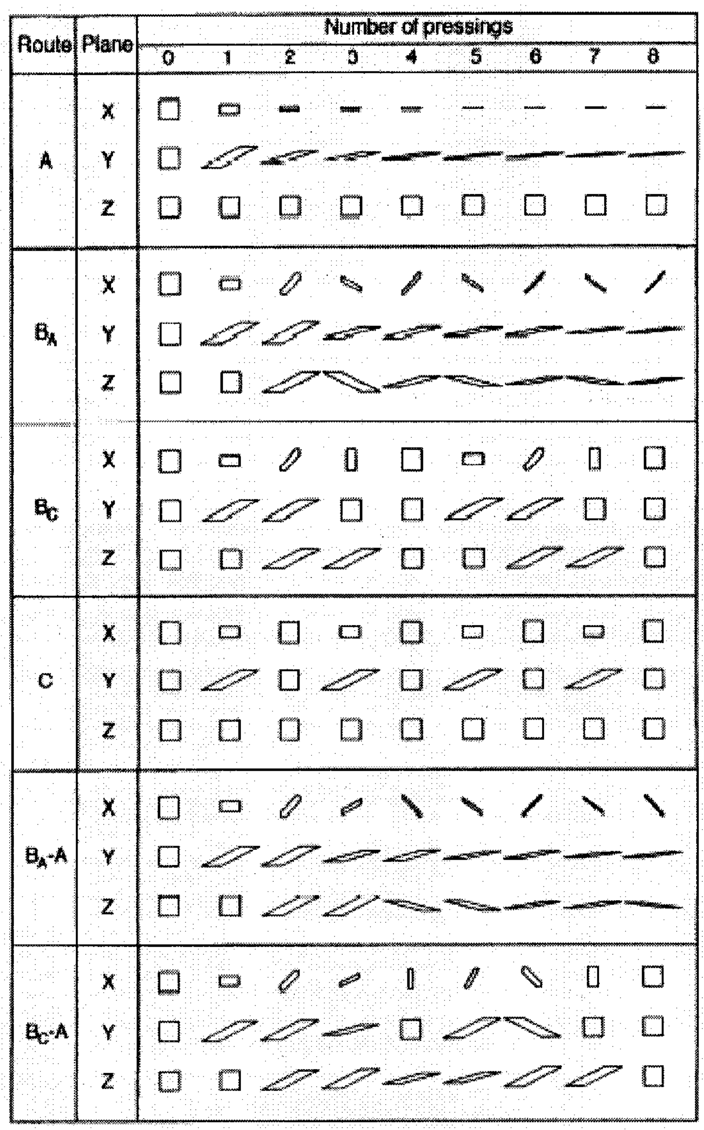

2.3. Microstructures, Mechanical Properties and Texture Development Produced by ECAP in Magnesium Alloys

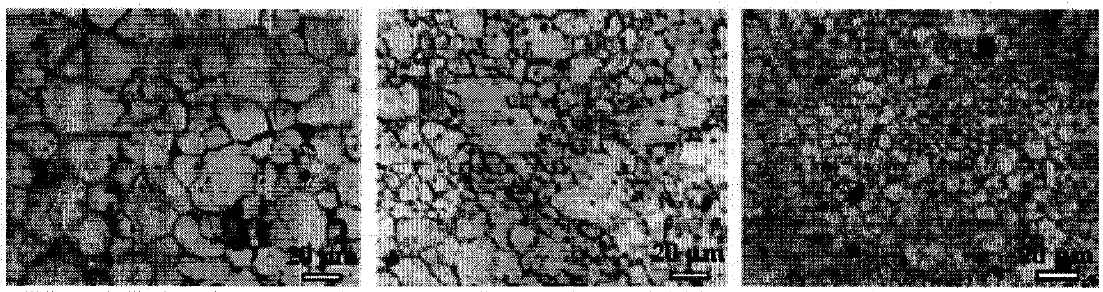

Figure 2.9. Microstructure of a) a conventionally extruded, b) a one-pass ECAP'ed sample, c) an eight-pass ECAP'ed sample of AZ61 alloy [25].

ECAP is successful in refining the grain size by recrystallization, resulting in a homogeneous, equiaxed grain structure. In so doing, it significantly improves both strength and ductility [26].

ECAP conducted with an extruded bar of AZ61 magnesium alloy with rotations of 90° always in the same direction (route B_C) for up to 8 consecutive passes produces a homogeneous fine-grained equiaxed structure (Figure 2.9). This indicates that recrystallization has taken place. In this case, ECAP was conducted in a 90° die at a temperature of 548K (275°C). The samples processed by ECAP were then annealed at 673K (400°C) to coarsen the grains before determining the mechanical properties in tension. By carrying out the tensile tests at room temperature using a strain rate of $5x10^{-4}s^{-1}$, it was found that the elongation-to-failure of the ECAP processed alloy was almost twice as large as that of the conventionally extruded starting material: 55% vs. 32% [25].

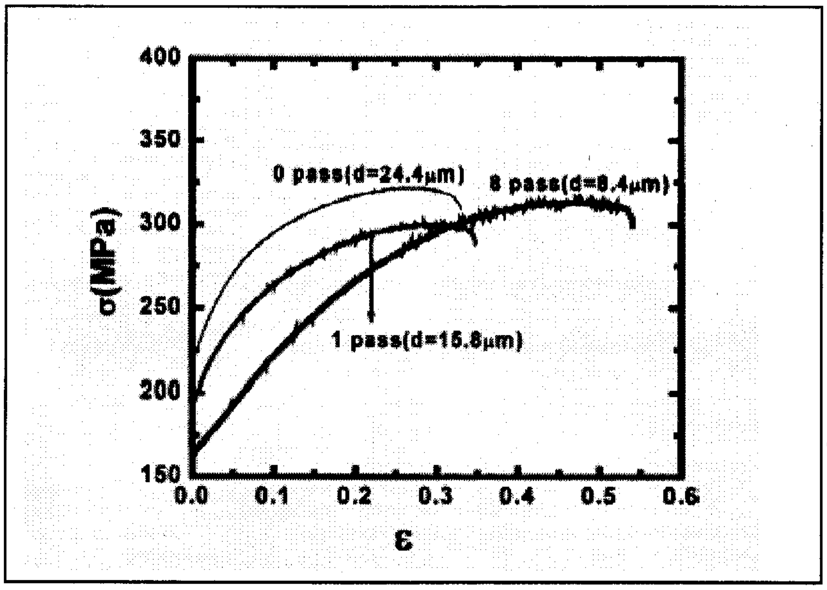

Figure 2.10. Engineering stress-strain relations for conventionally extruded, one-pass and eight pass ECAP samples of the AZ61 magnesium alloy [25].

The same can be said for the AZ31 magnesium alloy. ECAP was conducted at a temperature of 473K and the samples were then annealed at 573K for 24 hours. Following tensile tests at room temperature using a strain rate of $1\text{x}10^{-3}s^{-1}$, it was also found that the elongation-to-failure of the ECAP processed alloy was twice as large as that of the conventionally extruded alloy: 47% vs. 23% [26].

Experiments carried out on an AZ61 magnesium alloy also showed grain refinement; however, the yield stress vs. $d^{-1/2}$ graph had a negative slope as seen in Figure 2.11. This can be explained by the gradual transition of the texture during repetitive ECAP to control the grain size.

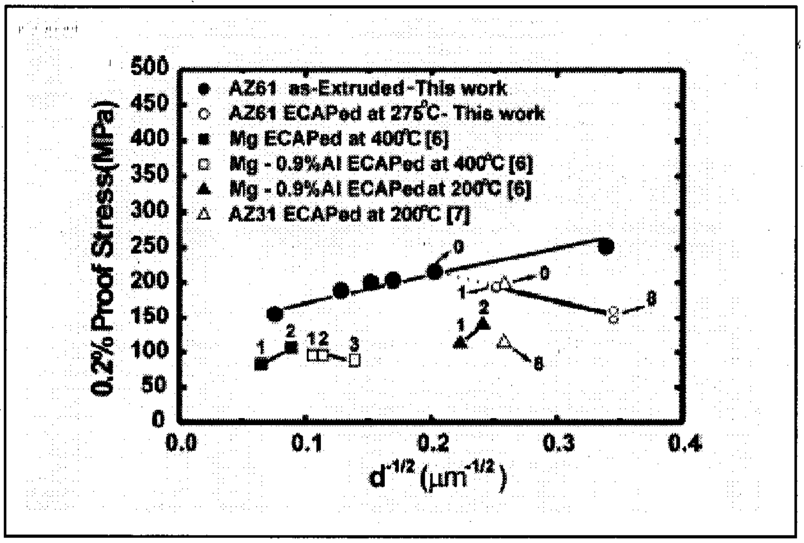

Figure 2.11. 0.2% proof stress plotted against $d^{-1/2}$ for conventionally extruded and ECAP processed AZ61 alloys along with data from Yamashita et al.[26] and Mukai et al. [16]. Numbers next to symbols indicate the number of pressings [25].

Most basal poles are rotated close to 45° from the extrusion and transverse directions after several ECAP passes. A lower applied stress is then needed to produce yielding on the basal planes following ECAP because this rotation of the basal poles to 45° from the extrusion axis causes the Schmid factor on the (0001) to increase [26]. However, this is not sufficient to explain the increase in ductility after ECAP; the large strain hardening along with the large ductility suggest that two or more additional slip planes have become activated, facilitating the texture transition during ECAP in this way [26].

2.3.1. Texture Observations

In an investigation carried out by Kim et al., the original fiber texture of the extruded alloy was gradually transformed into a new texture as a result of the repetitive pressings. The B_C and A routes yielded the dominant textures after 8 passes of $(10\bar{1}1)[0\bar{1}11]$ +$(10\bar{1}2)[\bar{1}2\bar{1}0]$ and $(10\bar{1}2)[\bar{1}2\bar{1}0]$, respectively, as seen in Figure 2.12 [22].

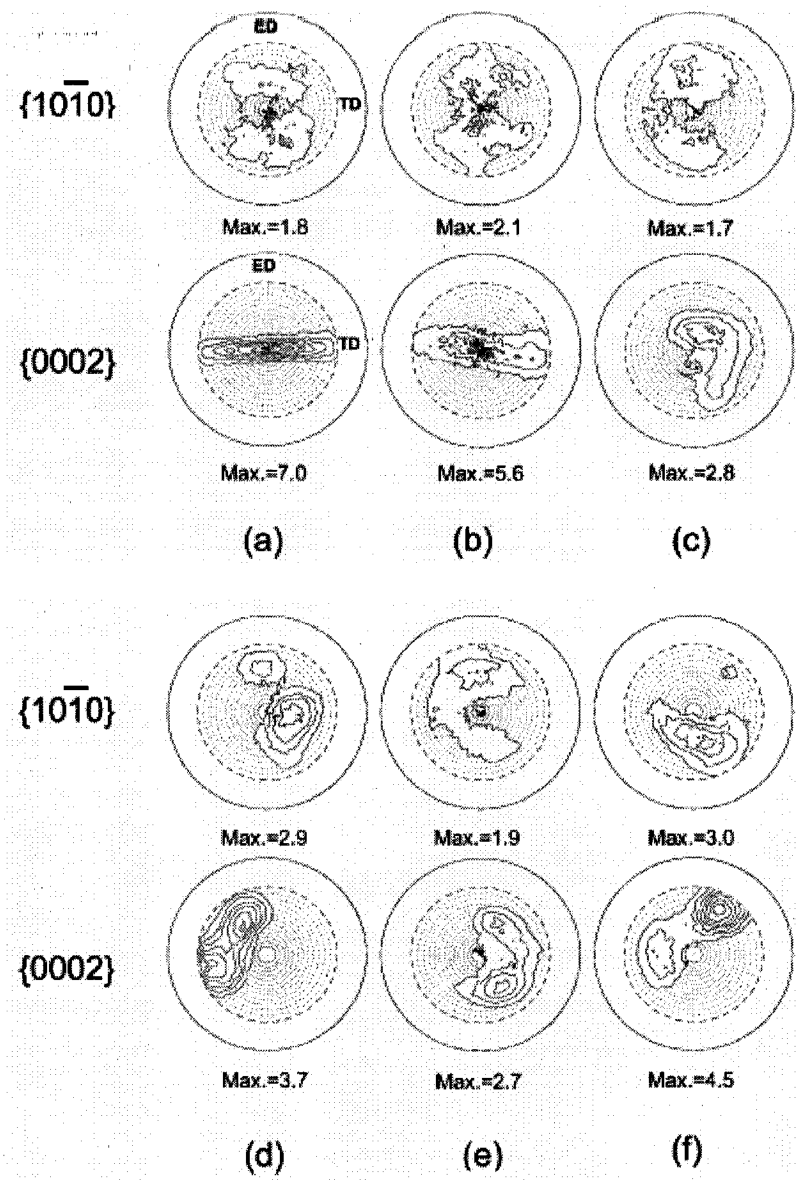

Figure 2.12. {10$\bar{1}$0} and {0002} pole figures of the AZ61 alloy a) 0 pass, b) 1 pass, c) 2 passes, d) 3 passes, e) 4 passes and f) 8 passes of ECAP processing following route B_C. [22]

For the B_C route, the yield stress decreased compared to that of the as-extruded material, because texture softening dominated over grain refinement. Following ECAP processing, the basal planes are more favourably oriented for slip and a lower applied stress is therefore needed to produce yielding on the basal plane. For the A route, the yield stress was slightly increased after 8 passes. The texture developed was different from that produced by the B_C route, orienting the basal planes somewhat unfavourably for slip. This again indicates that ductility in ECAP-processed magnesium alloys requires the activation of two or more slip planes during subsequent tensile testing [22].

In recent work reported by Koike *et al.*, samples were observed using a TEM; this revealed that, by the time 2% elongation is reached, there has been substantial dislocation activity on the non-basal planes. Further analysis indicated that dislocation cross-slip to non-basal planes occurred at a yield anisotropy value of 1.1 as opposed to the expected value of 100. The activity on the non-basal slip systems was attributed to grain-boundary incompatibility stresses. At 16% elongation, the sample exhibited twin formation and the strain was relaxed in some twins as well as in some untwinned areas. It was concluded that dynamic recovery occurs at room temperature. The large tensile ductility of the ECAP-processed AZ-31 magnesium alloy was attributed to the activity of the non-basal slip systems and to dynamic recovery. It was considered that these new deformation mechanisms are not only limited to ECAP-processed magnesium alloys but also to fine-grained magnesium alloys processed by other techniques [28].

ECAP performed on conventionally extruded AZ31 magnesium alloy for 8 passes, using route B_C, showed that the deformation texture became stronger than the original texture (Figure 2.13). There is a preferred orientation, with the basal planes inclined at 45° to the bar axis, as was found for the AZ61 alloy. Samples containing these textures had good room temperature ductility, combined with low yield stresses and good hardening responses; this gives magnesium alloys the potential for excellent formability.

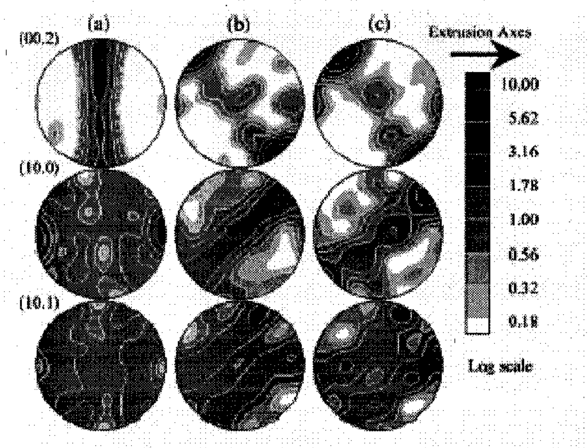

Figure 2.13. Pole figures showing crystallographic textures in a) conventionally extruded, b) 8-pass ECAP processed (using B_C), and c) ECAP processed (using B_C) and annealed samples [27].

However, the plastic response was highly anisotropic and some directions of loading actually exhibited significantly lower ductilities than the conventional material. Both the plastic anisotropy (yield stress and hardening behaviour) and aspects of the anisotropy in their fracture ductility can be rationalized in terms of the strong crystallographic texture induced by the ECAP process [27].

Another study using rolled AZ31 with a rolling texture as the initial material and processing it for 1 pass at 250°C at 10 mm/min resulted in grain refinement from 25-30mm to a relatively homogeneous structure of approximately 7mm [29]. As a consequence of the shear deformation, the grains were found to rotate so that the c-axis became aligned with the z direction. This can be seen in Figure 2.14 in the (0002) pole figure, where two maxima form at approximately ϕ=25° to the x axis and 75° to the z axis after one pass [29].

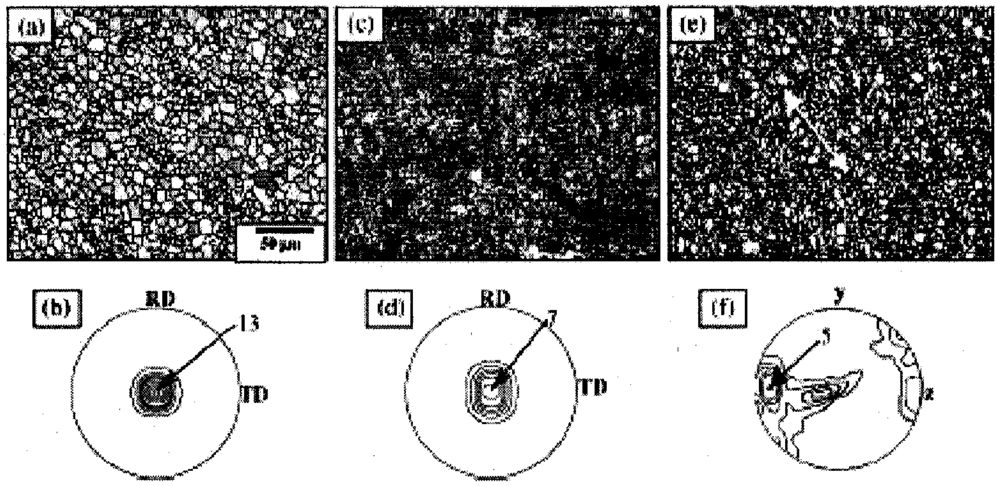

Figure 2.14. Microstructures and (0 0 0 2) pole figures of AZ31 material: (a) and (b) as-received (rolling plane, RD is vertical), (c) and (d) rolled at 375°C (rolling plane, RD is horizontal) and (e) and (f) after ECAP at 250°C (plane YZ, *y* is horizontal). The arrow indicates the shear direction during ECAP [29].

Agnew *et al.*, who used several conventionally extruded and one as-cast commercial magnesium, maintain that, regardless of processing route, ECAP will produce a certain class of textures defined generally as <0001> fiber textures. The orientation of the <0001> fiber texture will depend on the alloying elements [30].

After 1 pass, AZ80 and AZ31 exhibit the same fiber texture with the c-axis approximately 20° from the extrusion direction (and to the right). This is as expected because it would place the basal planes nearly parallel to the shear plane [32]. Subsequent route A passes continue to strengthen this texture, reorienting it to a similar texture after each subsequent pass [30]. Route B results in a strengthening of the texture, the peak intensity in the basal pole figure is at its highest at 50° and 60° from the extrusion direction, as seen in Figure 2.15.

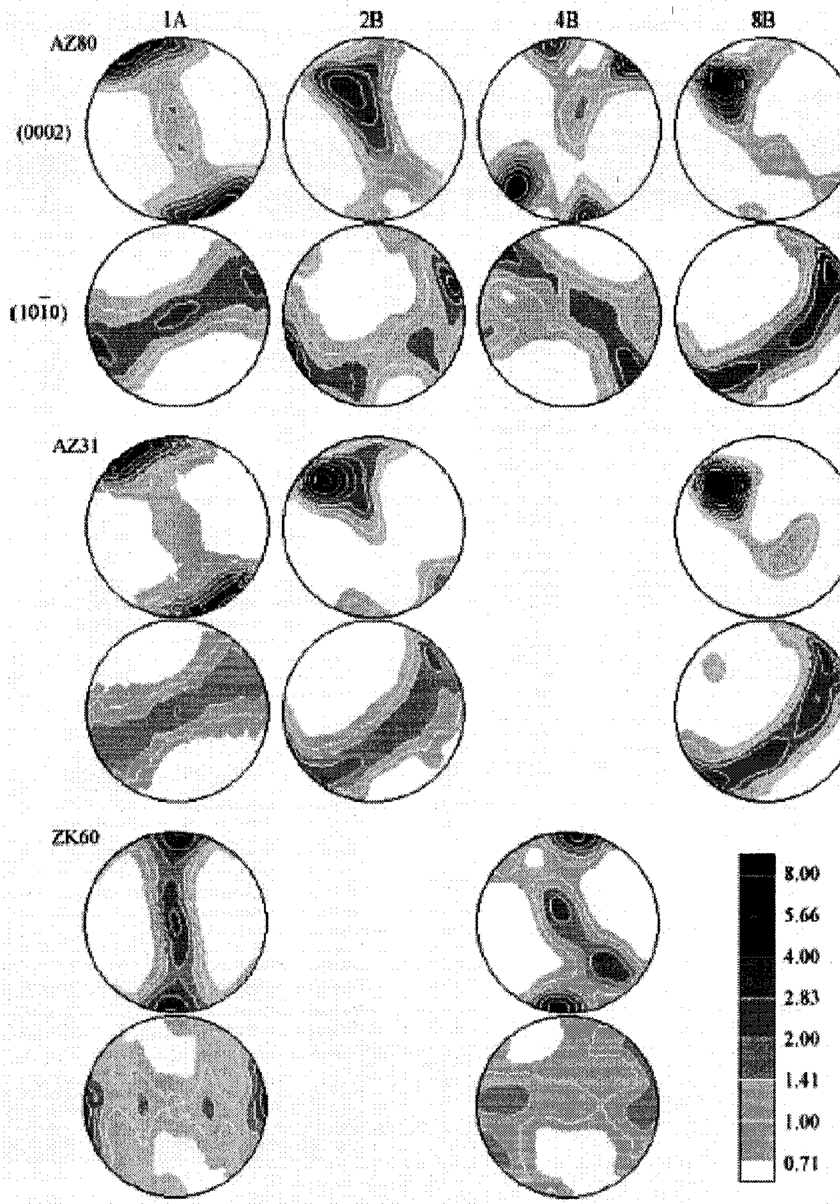

Figure 2.15. (0 0 0 2) and (1 0 $\bar{1}$ 0) pole figures showing textures after processing by ECAE for 1 pass and 2, 4 and 8 passes by route B for alloys AZ80, AZ31 and ZK60 [31].

For the ZK60 alloy, the two major differences are that after 1 pass, the <0001> fiber is oriented closer to the vertical axis and a secondary <0001> fiber is stabilized at the flow plane [31].

Comparing the extruded and as-cast AZ31 texture evolutions, it is evident that the initial texture and grain size do not make large contributions. Comparing this with the route B evolution (Figure 2.16), it is obvious there is much similarity with route C (Figure 2.17). It is possible to see that a single dominant <0001> fiber texture is developed and, depending on the alloying elements, for example, AZ alloys will develop a fiber texture inclined at 55° while the ZK alloy develops a fiber texture closer to 90° to the extrusion axis [31].

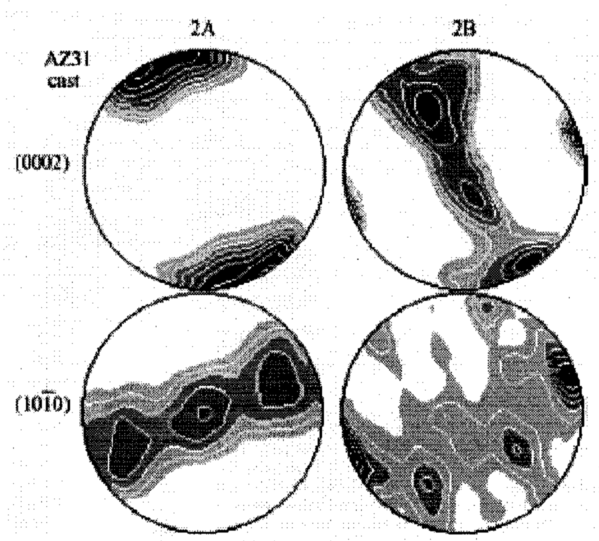

Figure 2.16 (0 0 0 2) and (1 0 $\bar{1}$ 0) pole figures showing ECAE textures from the initially as-cast AZ31 after two passes by routes A and B, respectively. The extrusion axis is to the right and the contour scale is shown in Figure 2.15 [31].

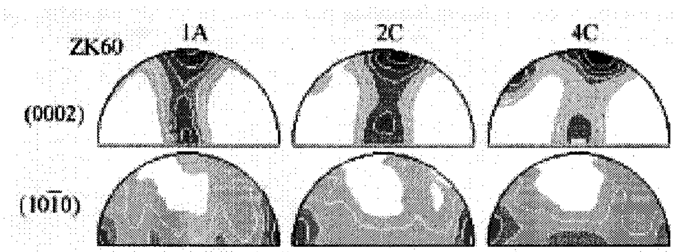

Figure 2.17. (0 0 0 2) and (1 0 $\bar{1}$ 0) pole figures (upper half) showing ECAE textures from alloy ZK60 after 1, 2 and 4 passes by route C. The extrusion axis is to the right and the contour scale is shown in Figure 2.15 [31].

Furthermore, inconsistencies in the textures for one sample but taken from different locations were recorded. This heterogeneity could be due to the possibility that the process imparts intrinsically non-uniform strain during a single pass or more likely that multiple passes of a short billet result in some 'end' effects, which can propagate into the bulk of the sample [33]-[35].

2.4. Superplasticity

As discussed above, magnesium alloys are the lightest structural metals and have many potential applications. They are ideal for structural components in aerospace applications because of their low density. However, due to their hexagonal closed-packed (HCP) crystal structure, they generally have poor workability. Nevertheless, the workability can be improved by refining the grain size and, if this is sufficient to allow superplastic forming, processing for practical applications may become possible.

Magnesium alloys can be rendered superplastic at relatively low temperatures by means of prior processing with ECAP. It has been proven to be effective in enhancing the mechanical properties at room temperature and producing superplasticity at elevated temperatures [26], as is the case for aluminum alloys.

2.4.1. Fundamentals of Superplasticity

Superplastic deformation refers to the ability of some metallic alloys to be extended to large tensile elongations before final failure [19]. For deformation in uniaxial tension, elongations to failure exceeding 200% usually indicate superplasticity, although several materials can reach extensions of over 1000% [36].

Superplasticity can be subdivided into two types: micrograin or microstructural superplasticity and transformational or environmental superplasticity. The latter is less significant from a commercial viewpoint and therefore microstructural superplasticity has been the subject of much more extensive work [36].

The two major requirements for microstructural superplastic deformation are a very fine and stable grain size, usually less than 10μm, and a relatively high testing temperature of around $0.5T_m$, where T_m is the melting point of the material in Kelvin. Superplasticity is a diffusion-controlled process, which is typically incompatible with fine grain sizes since grain growth occurs at elevated temperatures in pure metals and simple solid solution alloys. Therefore optimal superplastic metals tend to be either: i) two-phase eutectic or eutectoid alloys, where grain growth is limited by the presence of two phases; or ii) alloys containing a fine dispersion of a second phase, which acts as a grain refiner [37].

While there is no unique rate-defining step controlling the mechanism of superplastic deformation, grain boundary sliding and grain rotation make substantial contributions to the total strain. The mechanical behaviour of superplastic materials is sensitive to both temperature and grain size. Temperature increase, or grain size decrease, will decrease the flow stress at the lower strain rates [38]. Superplastic deformation is characterized by low flow stresses. This, combined with the high uniformity of plastic flow, makes it of commercial interest for the superplastic forming of components.

2.4.2. Superplasticity in Magnesium Alloys

It has been shown that the elongation to failure of AZ31 magnesium alloy can be effectively enhanced by two-stage deformation. The first stage is carried out under dynamic recrystallization conditions so as to produce fine equiaxed grains. The second stage at higher temperature is designed to achieve maximum elongation to failure from the fine-grained structure. The recrystallized grains can then deform by grain boundary sliding and contribute to overall strains of 74-76% [39].

An extruded AZ61 magnesium alloy with a grain size of 17μm was found to exhibit superplastic behaviour in the low strain rate range displaying a maximum elongation of 461% at 648 K (375°C) and 3x 10^{-5} s^{-1}. The dominant deformation mechanism was grain boundary sliding in this case [40].

An AZ91 material was solution treated at 688K for 2h, followed by conventional extrusion at 523K with a reduction ratio of 4:1 [24]. It was then processed by ECAP at 448K to a total strain of 8.05. This alloy was subsequently used for tensile testing, carried out in the strain rate range 2 x 10^{-5}-$1x10^{-3}s^{-1}$and at a temperature of 473K in air. A large elongation of 661% was achieved at this relatively low temperature of 473K [41], as seen in Figure 2.18.

AZ91 was also investigated at 573 K and a strain rate of $1.5x10^{-3}$ s^{-1} During tensile deformation, grain refinement was observed and attributed to dynamic recrystallization. Grain boundary sliding also occurred due to the grain refinement and the result was an elongation to failure of 604% [42]-[43].

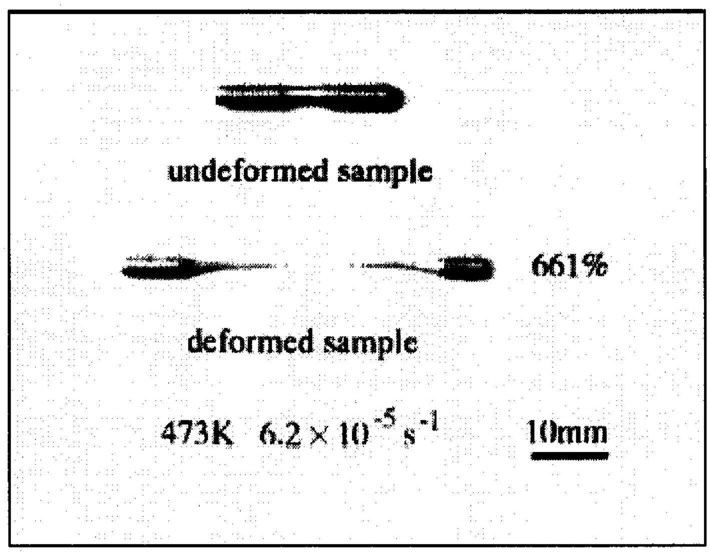

Figure 2.18. AZ91 magnesium alloy exhibiting superplasticity [41].

In an investigation carried out by Matsubara *et al.* [44], the ductility of a magnesium alloy containing 9wt.% Al was compared for the: i) as-cast, ii) conventionally extruded, and iii) ex-ECAP processed cases. Conventional extrusion was carried out at 623K at a rate of 5mm/s to a final reduction ratio of 36:1. The grain size measured for the conventionally extruded alloy was approximately 12μm. This extruded alloy was also used to produce the ECAP specimens and ECAP was conducted at 473K for 1 or 2 passes or 573K for a maximum of 4 passes in a 90° die at 8mm/s. Microstructural observation and tensile testing followed. While the as-cast alloy exhibited limited ductility and the conventionally extruded alloy displayed only moderate improvement, the ex-ECAP material was characterized by excellent superplastic ductilities. By testing this alloy over a range of temperatures and strain rates, it was shown that it is capable of producing both low temperature superplasticity with an elongation of 800% at 423K using a strain rate of 1×10^{-4} s^{-1} and high strain rate superplasticity with an elongation of 360% at 498K at a strain rate of 1×10^{-2} s^{-1} [44].

CHAPTER 3 - EXPERIMENTAL PROCEDURE

3.1. Material

The magnesium AZ-31 alloy was received in both as-cast and extruded form with the following composition:

Element	Al	Zn	Mn
Content (wt. %)	2.8	1	0.1

The as-cast ingots had the following dimensions d = 74 mm; h = 89 mm and the extruded rods d = 25 mm; h = 200 mm.

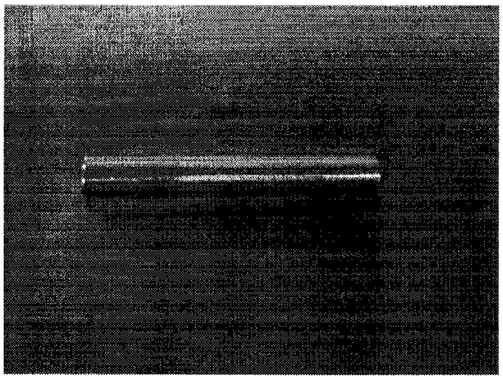

Figure 3.1. Macrograph of an ECAP specimen.

Both the as-cast ingots and the extruded rods were received and machined into cylindrical bars with the following dimensions: d = 11.8 ± 0.05 mm; h = 50 ± 2 mm. An example is shown in Figure 3.1.

3.2. Heat Treatment

The extruded alloy samples were placed on refractory bricks to be as close as possible to the thermocouple. This was done to promote accurate temperature measurement; the rods were placed a centimeter apart to allow air circulation.

The furnace was then turned on and the samples were allowed to heat up to temperature before the annealing time was set. Annealing was performed at 350°C for 1 hour and the samples were allowed to cool to temperature in the furnace.

3.3. ECAP

The ECAP machine employed an Instron equipped with a steel ECAP die containing a circular channel. It was connected to a heating element and a thermocouple. The latter was used to monitor the die temperature. The equipment is located at the Katholicke Universiteit Leuven in Leuven, Belgium, and the author is indebted to Professor Bert Verlinden for permission to use this apparatus.

The samples were coated with a molybdenum disulphide lubricant before being inserted into the die, where they were allowed to heat up to the testing temperature for approximately 10 minutes before every pass. At the end of the last pass the samples were quenched to room temperature in a water bath.

NOTE: Because of the design of the ECAP set-up, all samples underwent automatic annealing at temperature following extrusion until the next sample was extruded and the preceding sample could be extracted from the heated die. That is, each sample was pushed out by the succeeding specimen.

For the as-cast material, tests were attempted at a speed of 10 mm/s at a temperature of 400°C for up to 2 passes. The temperature was then increased to 450°C and the speed reduced to 2 mm/s and then further to 1 mm/s.

The trials were run at two temperatures, 250 and 300°C, using three routes A, B_C and C, at a speed of 5 mm/s for up to 8 passes. One trial was carried out at 200°C and a decreased speed of 1mm/s.

3.4. Sample Preparation

The samples were then cut along their longitudinal axes for examination of the microstructures, see the plane shaded in grey in

Figure 3.2. The samples were cold mounted in epoxy and ground with silica sandpaper from 600 to 800 to 1200 grit and then polished with a diamond suspension of 3μm. Half of each sample was reserved for mechanical testing and a cylindrical sample was machined along the extrusion axis for compression testing.

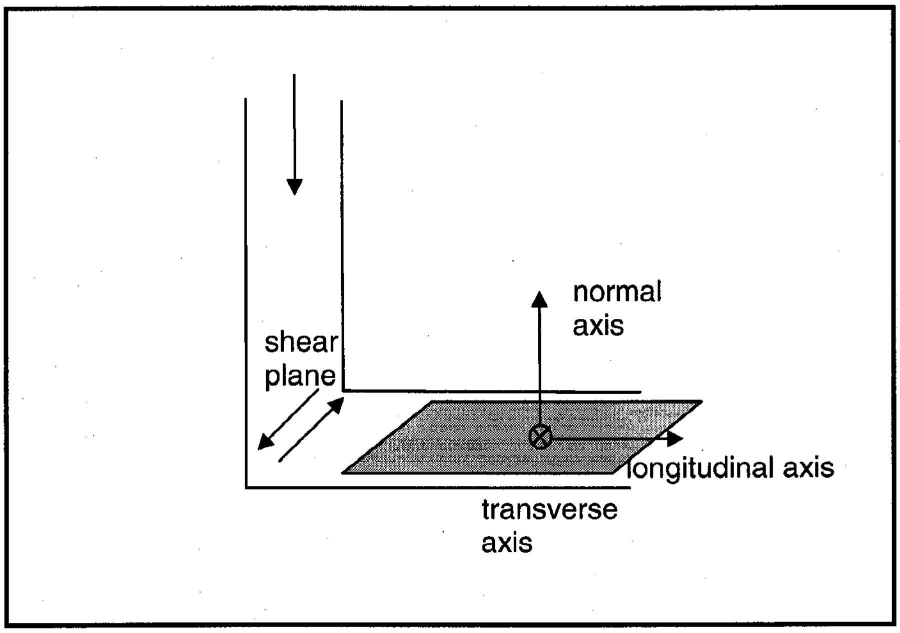

Figure 3.2. Schematic of the plane of microstructural examination with respect to the specimen in the die.

3.5. Microstructural Examination

The samples were chemically polished using a 10% nital solution for approximately 30 seconds and then etched to reveal the microstructure using the following solution:

4.2g of picric acid
10 ml of acetic acid
10ml of distilled water
70ml ethanol

This etch was performed 'instantaneously' (~1 second) and the sample was then washed with ethanol. The etching step was repeated if needed. Examination was performed on an Epiphot 200 Nikon Optical Microscope and the micrographs were taken with a Clemex Image Analyzer.

3.6. Texture Measurement by X-Ray Diffraction

The crystallographic texture was measured by X-ray diffraction in a Siemens D500 goniometer system. The X-ray radiation used was molybdenum K_{α}. Corrections for peak defocusing and background intensities were made by measuring pole figures from a slightly compressed powder sample. The measured incomplete pole figures were obtained from the (0002), $(10\bar{1}0)$, and $(10\bar{1}1)$ Bragg peaks. The data were then analyzed using the ADC (Arbitrarily Defined Cells) method with the TexTools 3.2 software to calculate the orientation distribution functions and the complete pole figures. For each pole figure, standard θ-2θ scans were run to obtain the exact positions of the peaks.

3.7. Mechanical Testing in Uniaxial Compression

Compression samples with the following dimensions were machined: d = 7.5 mm; h = 11.4 mm. They were taken as close as possible to the center of the ECAP samples. The compression tests were performed at 200°C at a strain rate of $0.001s^{-1}$ up to a total strain of 80%.

CHAPTER 4 - RESULTS

4.1. Microstructural Analysis

4.1.1. ECAP Processing of the As-cast Material

The as-cast microstructure was found to have a large grain size, approximately 1 mm, with precipitates located along the grain boundaries, as seen in Figure 4.1.

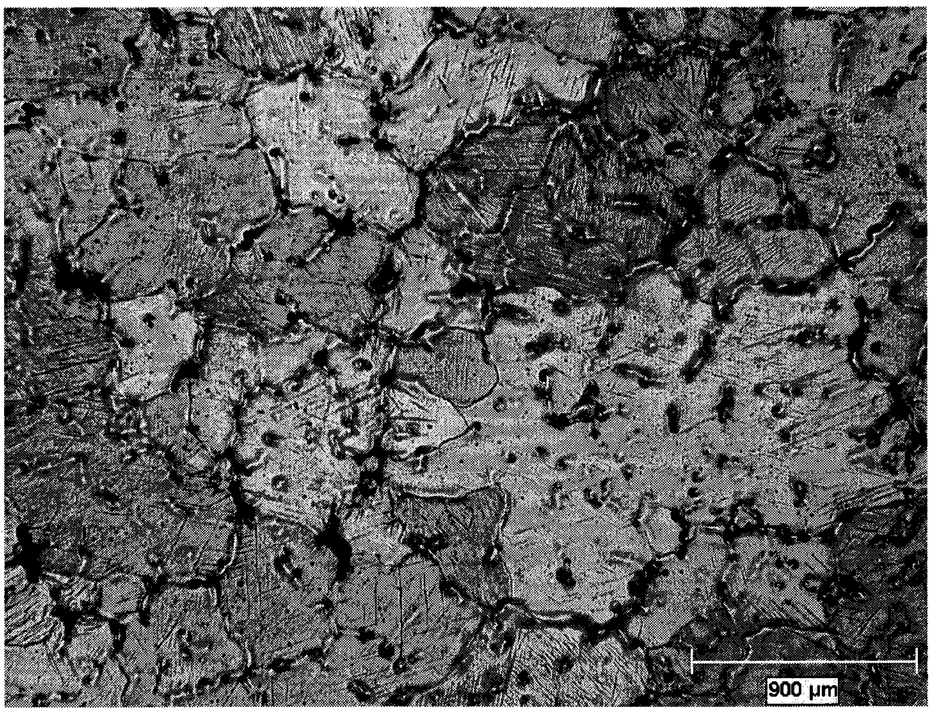

Figure 4.1. Microstructure of the as-cast AZ31 magnesium alloy showing the coarse grains (~ 1mm) and the grain boundary precipitates.

The following samples were successfully processed using the as-cast material at a speed of 10 mm/s:

Route	T(°C)	Passes
A	450	1
A	450	1 and 2

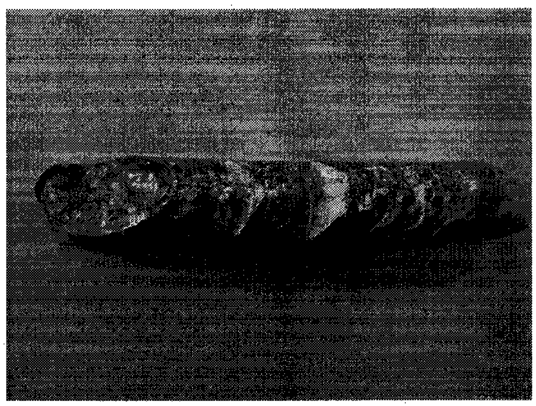

(a)

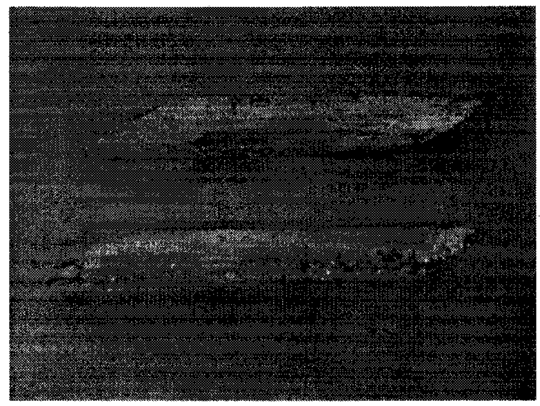

(b)

Figure 4.2. Macrographs showing samples following ECAP at (a) 400°C and (b) 450°C.

As-cast samples run at 400°C had severe cracks, as shown in Figure 4.2 (a). The operating temperature was increased to 450°C and the speed was decreased to 2mm/s and the sample obtained was much improved, as seen in Figure 4.2 (b). The speed was then further decreased to 1mm/s and subsequent samples were further improved. A two-pass sample was then produced with the first pass pressed at 1mm/s and the second pass at 2mm/s.

At this point it became apparent that the incipient melting occurring at the relatively high operating temperatures used to improve the formability of the as-cast material would inhibit further experimentation. After the first pass, there remained large elongated grains but there were also smaller grains surrounding the larger grains, as shown in Figure 4.3 (a). The second pass achieved a fine, uniform and equiaxed grain structure, compare Figures 4.3 (a) and (b).

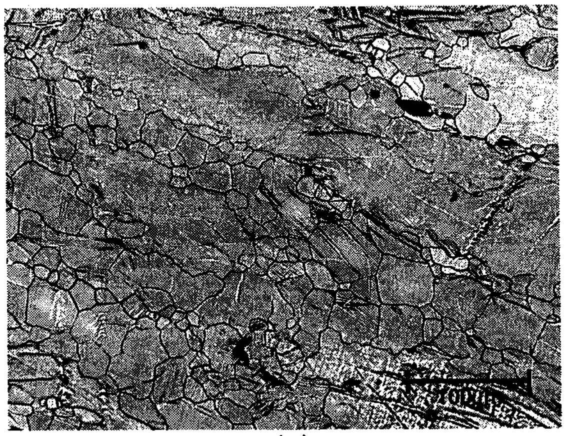

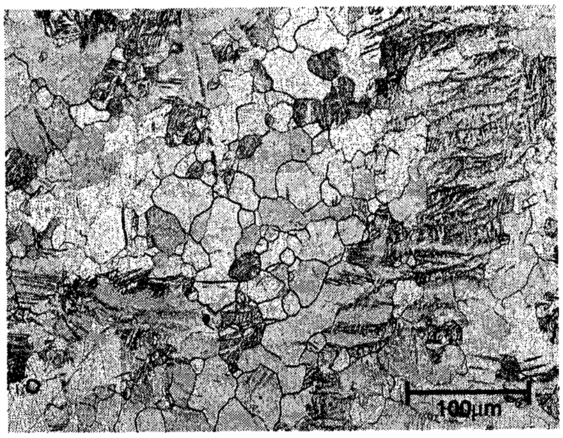

(a) (b)

Figure 4.3. Microstructures of as-cast ECAP samples processed by route A at 450°C, (a) 1 pass and (b) 2 passes.

While annealing might have improved the properties of the starting material, to ensure optional conditions subsequent experiments were undertaken with extruded material.

4.1.2. ECAP Processing of the Extruded Material

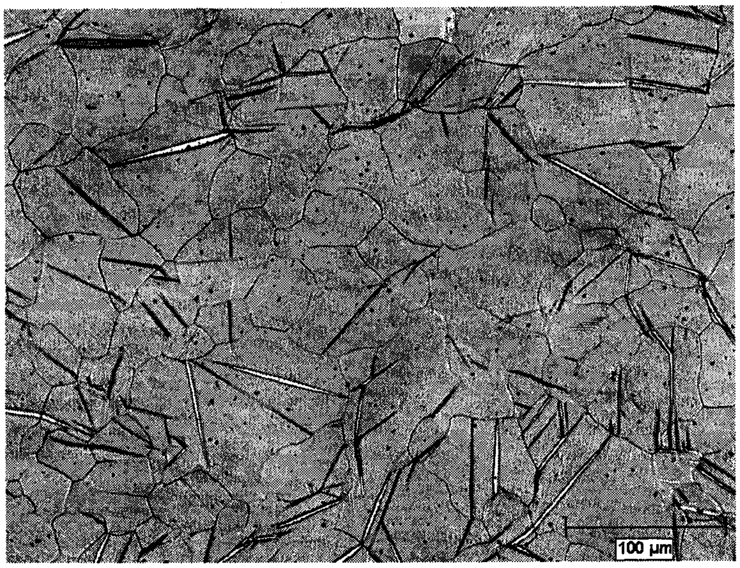

Figure 4.4. Microstructure of the extruded AZ31 magnesium alloy displaying a grain size of ~ 50μm. Here the extrusion direction is normal to the surface.

Conventional extrusion results in a grain size of approximately 50 μm, displayed in Figure 4.4, which is finer than that of the as-cast alloy. These are equiaxed because of recrystallization, static or dynamic or both. There are no longer any precipitates and extension twins can be observed throughout the microstructure. The trials at 250 and 300°C were successful at 5 mm/min; however, at 200°C, the sample exhibited severe cracking parallel to the shear plane, as illustrated in Figure 4.5 (b). Only a single successful 1-pass sample was produced at 200°C using a speed of 1 mm/min.

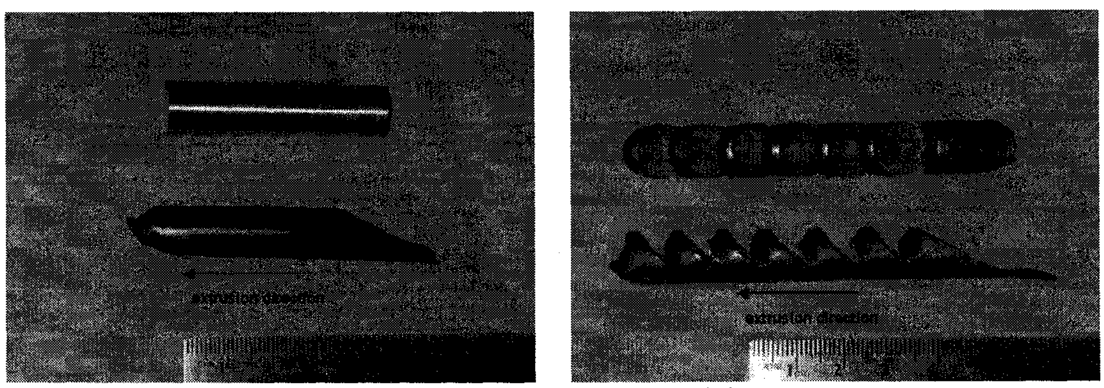

(a) (b)

Figure 4.5. Macrograph showing ECAP samples before and after pressing (a) 1 pass at 250°C and (b) 1 pass at 200°C.

Samples were successfully produced using the extruded material under the following conditions:

Route	T(°C)	Passes
A	200	1
	250	1,2,4,8
	300	1,2,4,8
B_C	250	1,2,4
	300	1,2,4
C	250	1,2,4,8
	300	1,2,4,8

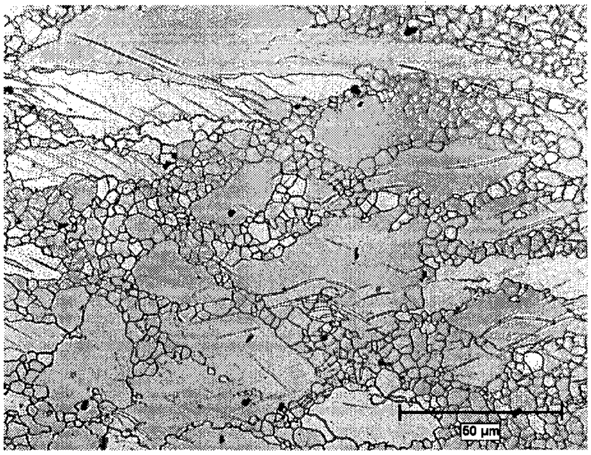

Figure 4.6. Microstructure of a 1-pass ECAP sample processed at 200°C showing the necklace effect that is typical of dynamic recrystallization.

After pressing at 200°C, an obvious necklace effect was observed in the microstructure, with very fine grains surrounding large grains, as seen in Figure 4.6. This type of microstructure is indicative of dynamic recrystallization.

When route A was employed at 250°C, large sheared grains remained after one pass and the microstructure became uniformly finer following two passes. However, further pressing did not produce any significant change in the microstructure, as seen in Figure 4.7.

Increasing the temperature from 250 to 300°C resulted in a coarser final grain size, as can be seen by comparing Figure 4.7 with Figure 4.8. After the first pass, no coarse grains remain and there is an evolution to a finer and finer microstructure after each pass. But the overall grain size in the eight-pass material is larger than that at 250°C.

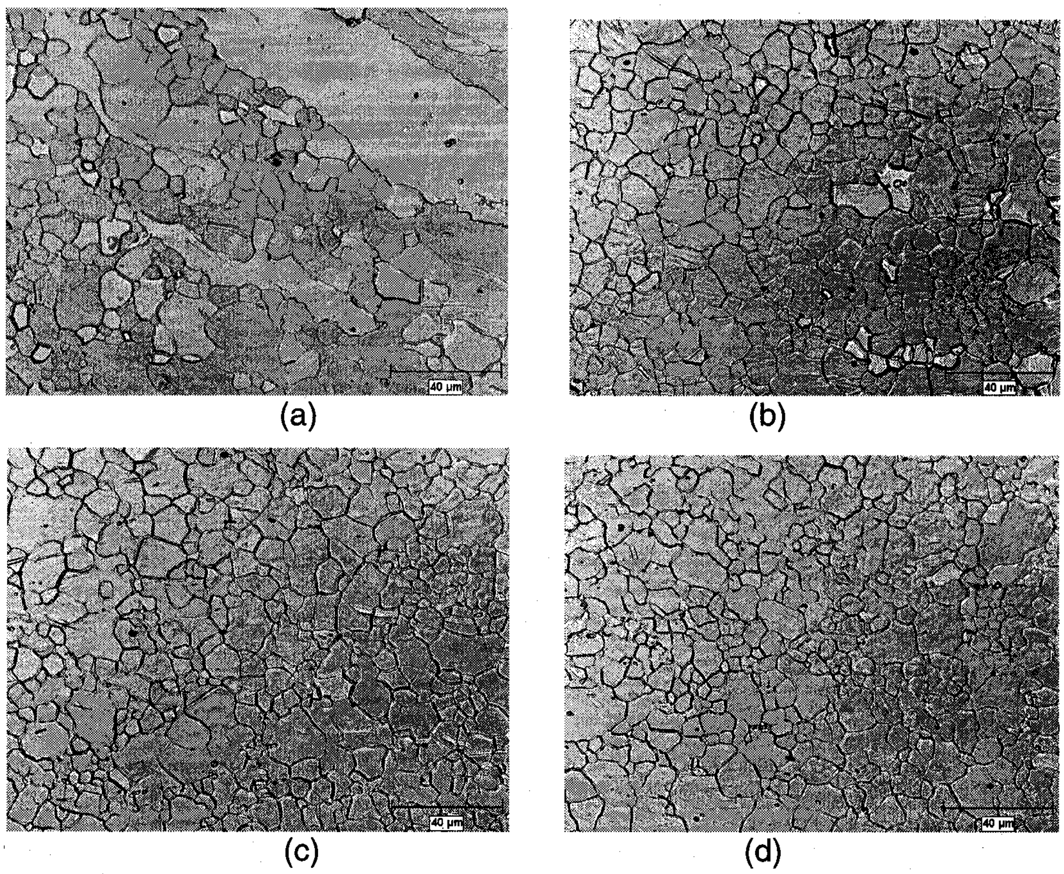

Figure 4.7. Microstructures produced at 250°C using route A (a) 1 pass, (b) 2 passes, (c) 4 passes, and (d) 8 passes (magnification 500x).

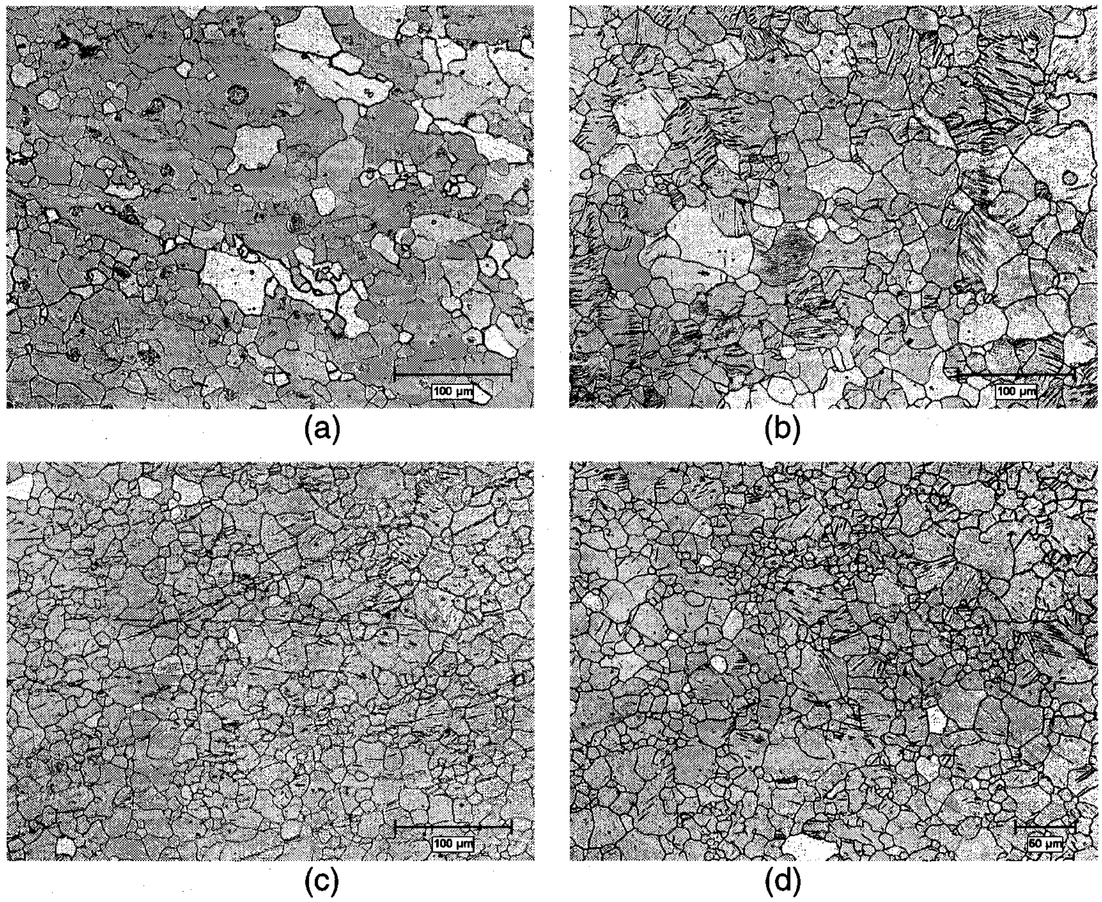

Figure 4.8. Microstructures produced at 300°C using route A (a) 1 pass, (b) 2 passes, (c) 4 passes, and (d) 8 passes (magnification 200x).

Using route B_C, as opposed to route A, at 250°C, it is possible to achieve further grain size reduction following the second pass. This results in a finer grain size at four passes for route B_C compared to route A; once again, increasing the temperature from 250 to 300°C, leads to a larger final grain size, as seen in Figure 4.9.

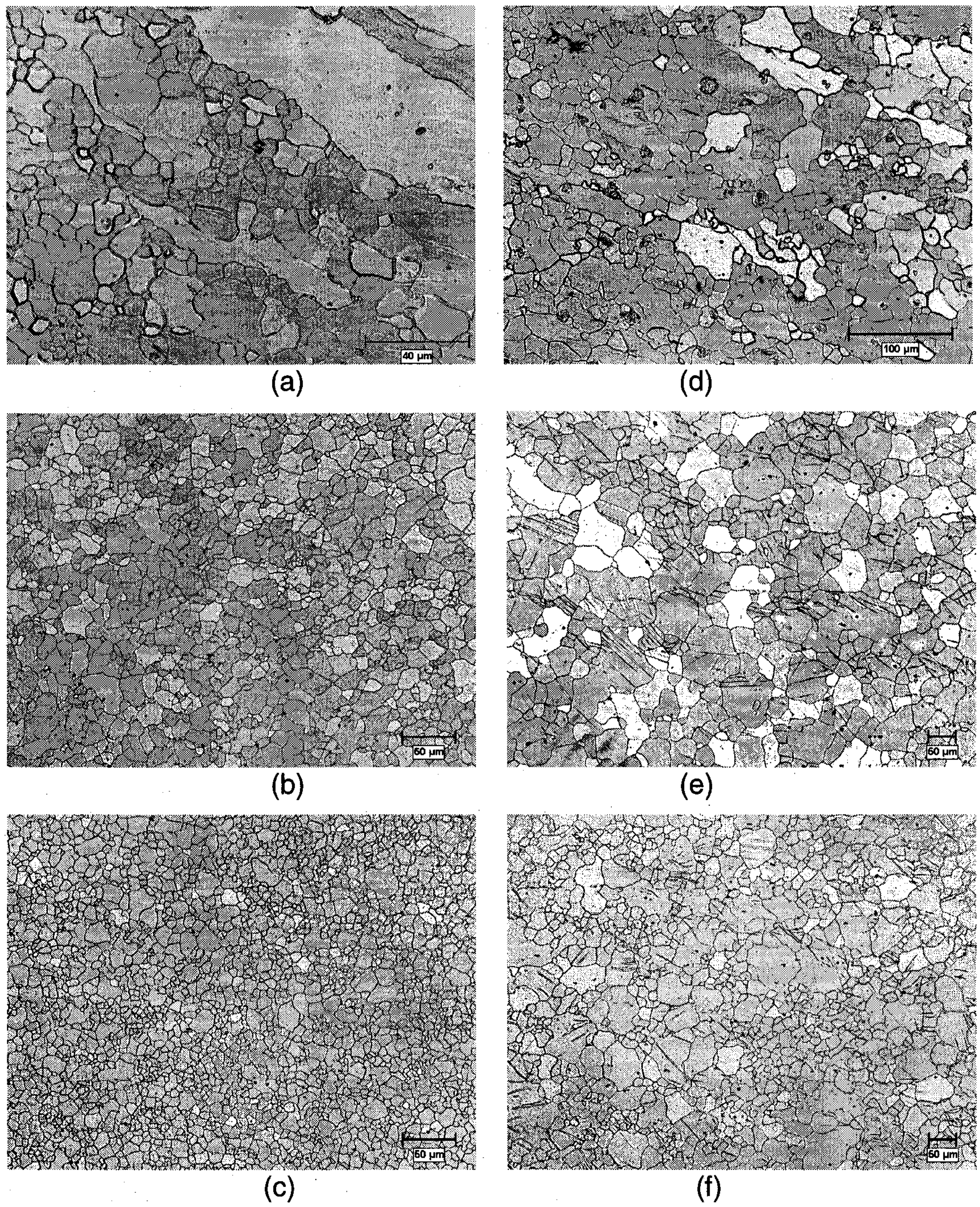

Figure 4.9. Microstructures produced at 250°C using route B_C (a) 1 pass, (b) 2 passes, (c) 4 passes, and 300°C (d) 1 pass, (e) 2 passes, (f) 4 passes (magnification 200x).

When route C was employed at 250°C, there was not much further reduction following the second pass. The general behaviour was similar to that observed using route A, as can be seen by comparing Figure 4.10 to Figure 4.7. Again for route C, increasing the temperature to 300°C increased the final grain size (compare Figure 4.11 to Figure 4.10). However, even at this temperature, it was possible to distinguish a slight refinement following the second pass.

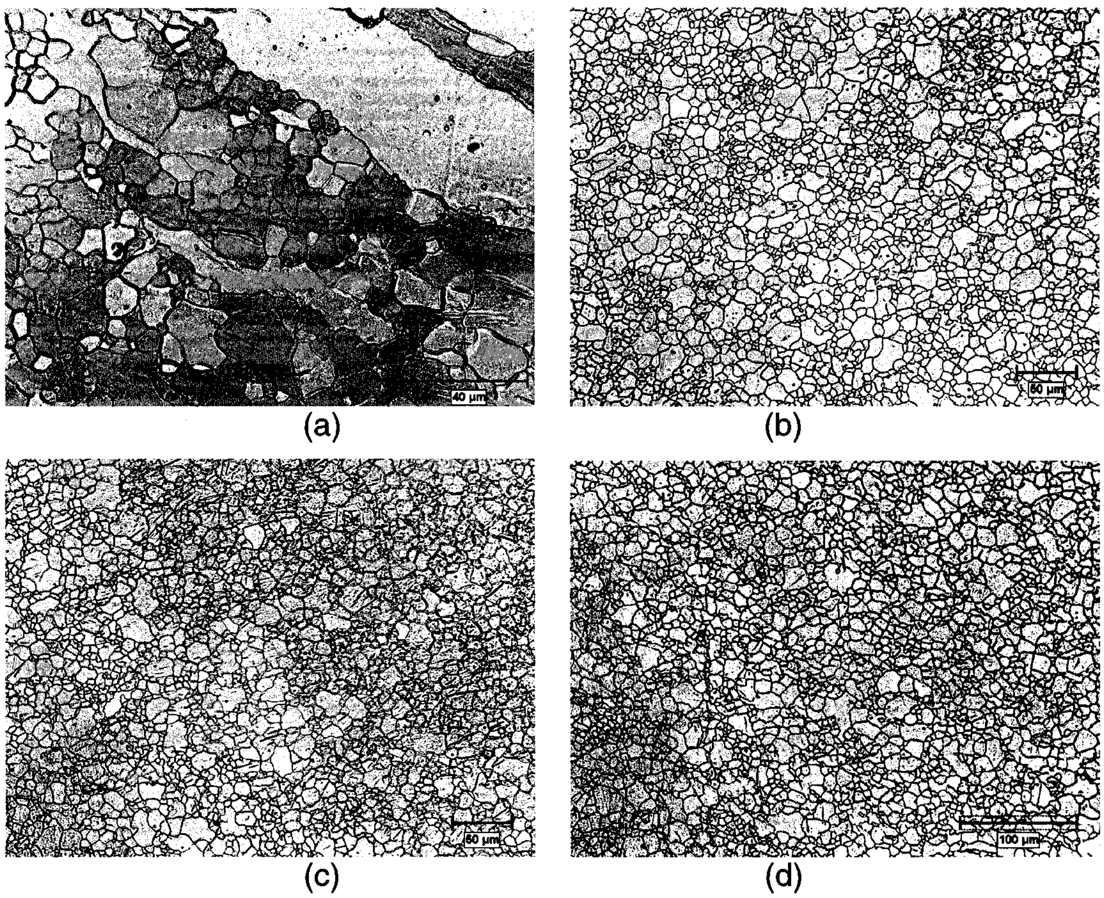

Figure 4.10. Microstructures produced at 250°C using route C (a) 1 pass, (b) 2 passes, (c) 4 passes, and (d) 8 passes (magnification 200x).

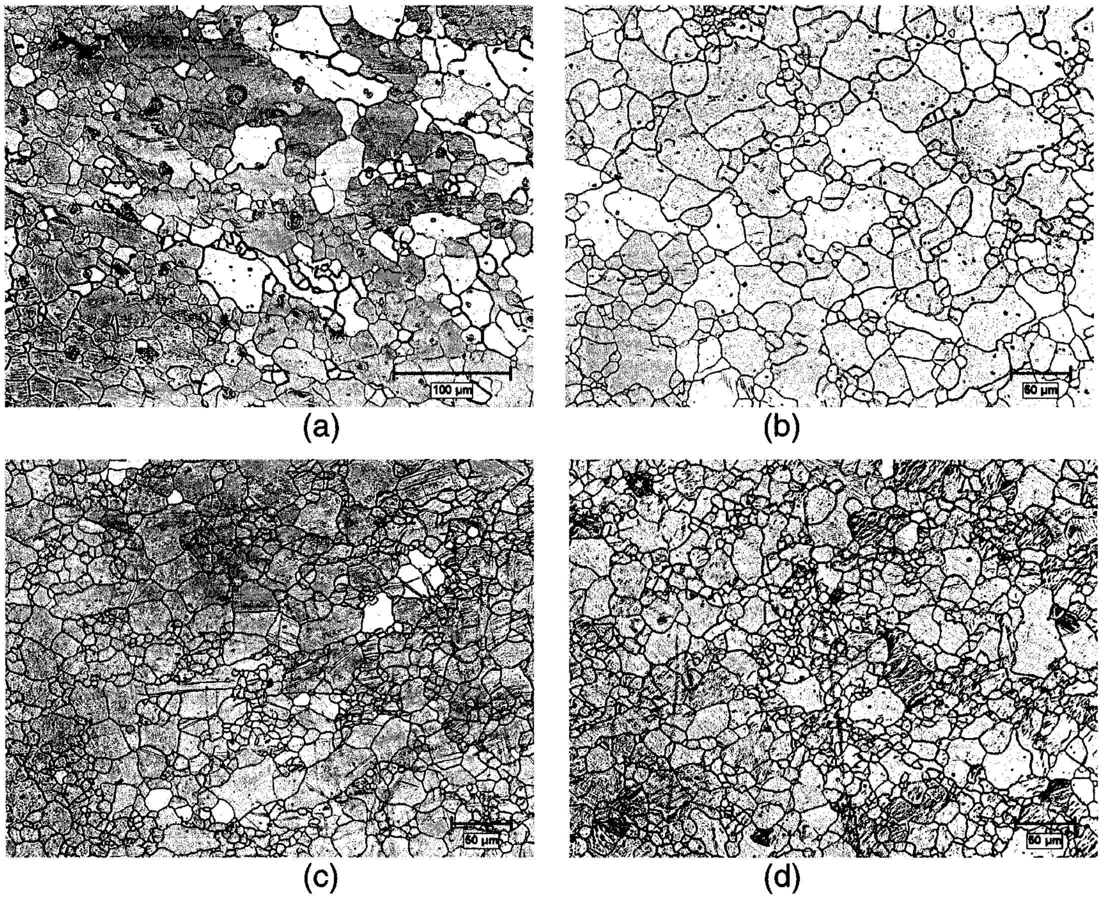

Figure 4.11. Microstructures produced at 300°C using route C (a) 1 pass, (b) 2 passes, (c) 4 passes, and (d) 8 passes (magnification 200x).

4.2. Texture Analysis

The initial material exhibited, as expected, an extrusion texture: i.e. the basal (0002) planes were aligned along the extrusion direction with their poles oriented all around the extrusion axis, as seen in Figure 4.12.

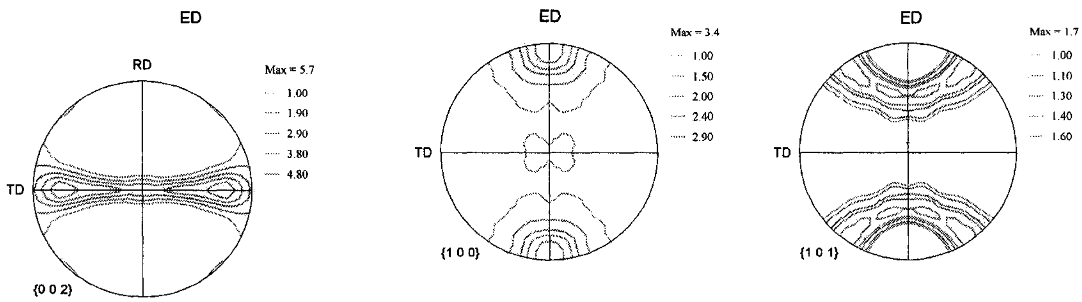

Figure 4.12. Pole figures of the initial texture of the as-extruded annealed AZ31 magnesium alloy.

Observing the effect of increasing ECAP temperature on the texture of the 1-pass material, it is clear that there is a change at 300°C, as illustrated in Figure 4.13.

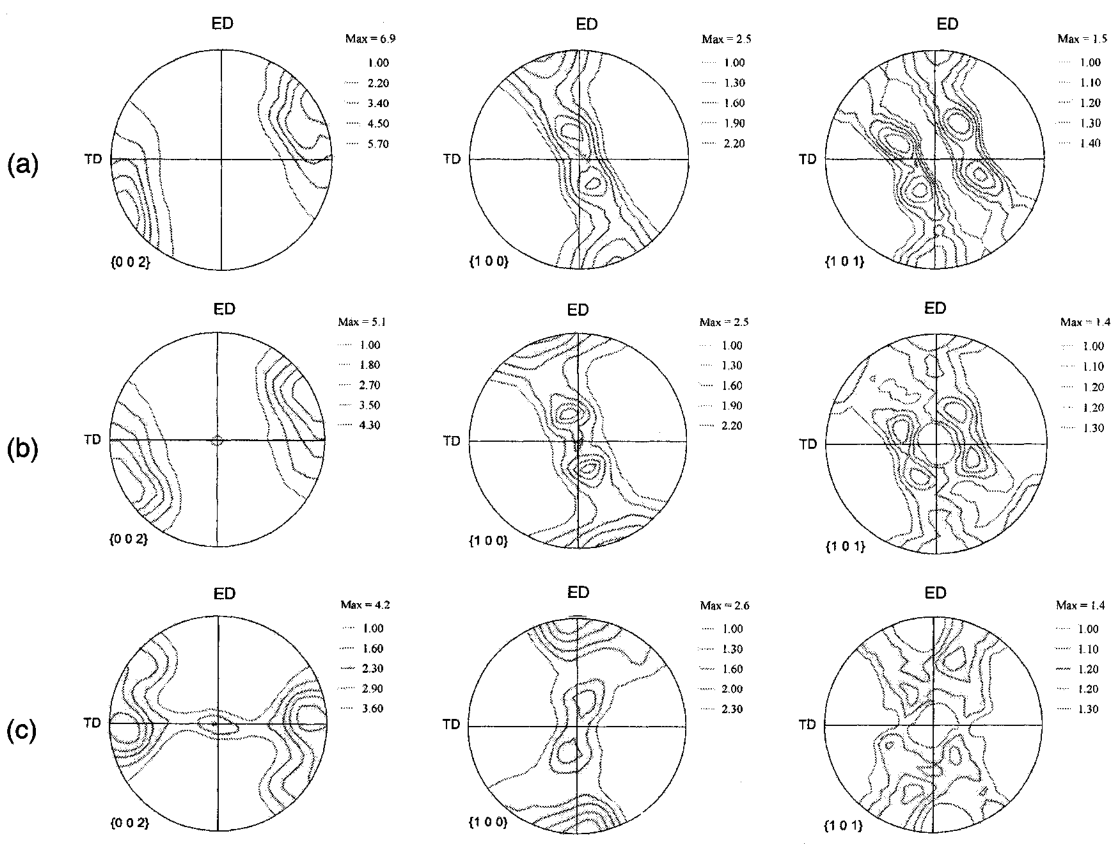

Figure 4.13. Pole figures for 1-pass route A samples processed at (a) 200°C, (b) 250°C and (c) 300°C.

The ECAP alloy processed through route A shows a 45° shift in the basal peaks after the first pass. As the number of passes increases, the peaks are rotated towards a rolling texture, with the basal poles oriented along the transverse direction, as seen in Figure 4.14. This is because the transverse direction corresponds to the "compression axis" in terms of the stress tensors (Figure 4.15).

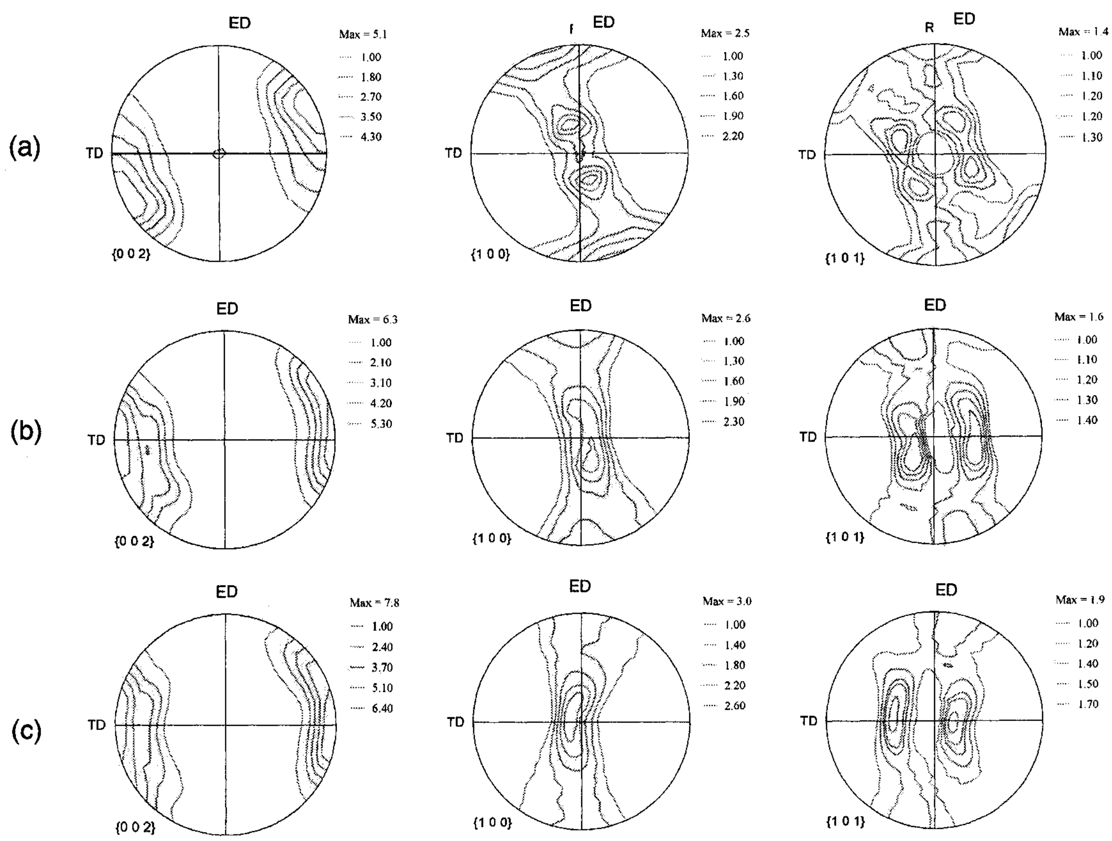

Figure 4.14. Pole figures for route A samples processed at 250° after (a) 1 pass, (b) 2 passes and (c) 4 passes.

For samples ECAP processed through route C, the 45° shift after the first pass is maintained after every pass, as seen in Figure 4.15. This is because the 180° rotation after each pass means that the shear plane (and therefore the shear texture) is established in *fresh material* after each pass.

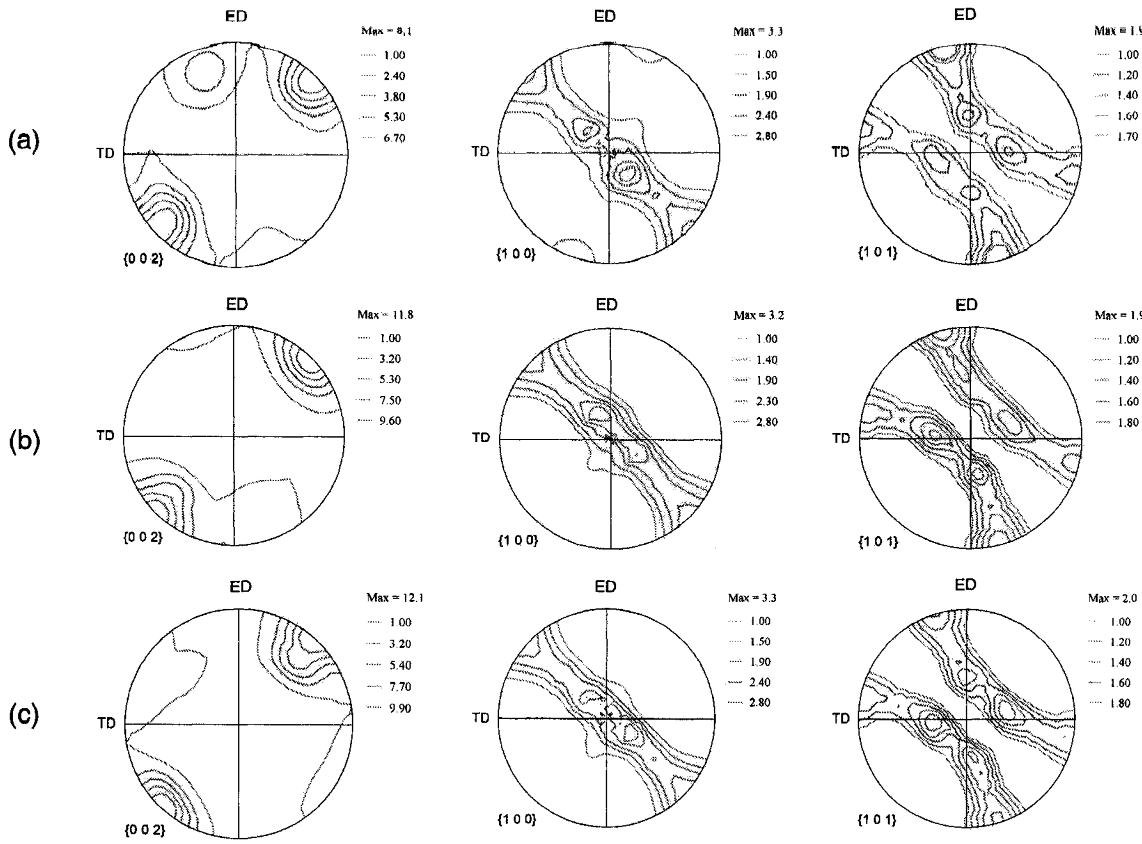

Figure 4.15. Pole figures for route C at 250°C after processing by (a) 2 passes, (b) 4 passes and (c) 8 passes.

4.3. Compression Flow Curves

During compression at 200°C, some of the samples underwent severe shearing along the ECAP shearing plane, as illustrated in Figure 4.16. It was also observed that shearing was more severe in the route C samples than in the route A samples. This is of course related to the texture differences depicted in Figure 4.14 and Figure 4.15.

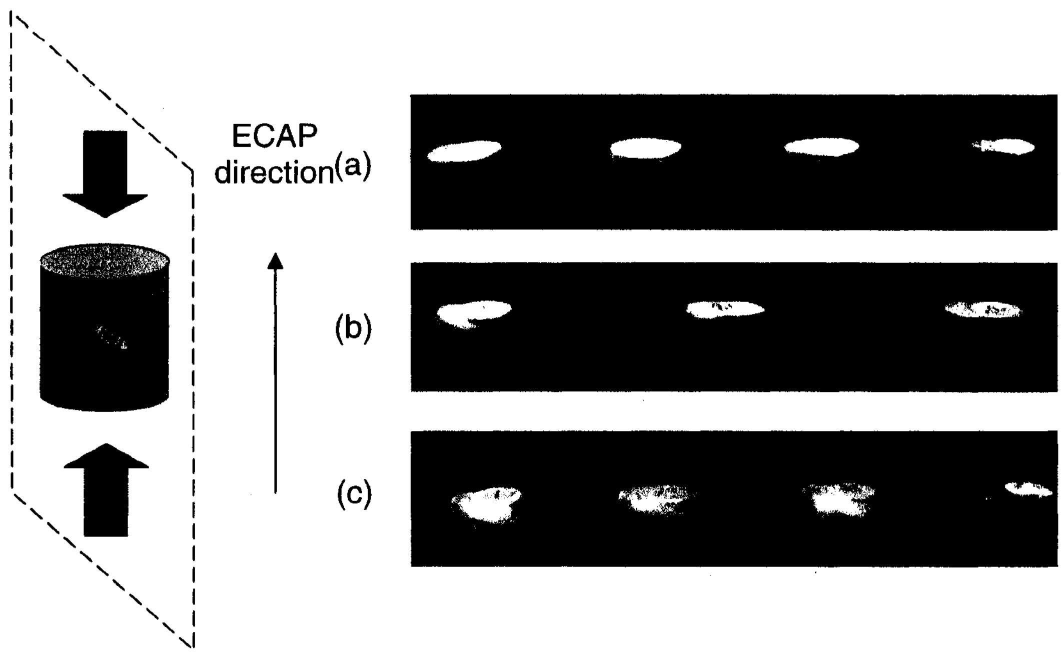

Figure 4.16. Schematic diagram showing the basal plane alignment within a compression sample with reference to the geometry of the original ECAP sample: (a) route A, (b) route B_C, and (c) route C samples.

Shearing took place at 45° to the compression axis, along the basal planes that were aligned as a result of ECAP processing. This caused slip to occur principally on these planes. Such ready shear led to highly localized flow.

The following graphs (Figure 4.17) show the effect of repetitive ECAP passes for routes A, B_C and C at 250°C. As the number of passes was increased, the strength decreased. This was probably associated with the progressive grain refinement produced by increasing the number of passes (see Figure 4.7 through Figure 4.11). The finer grains, in turn, increased the contribution of grain boundary sliding to the strain and reduced the flow stress in this way.

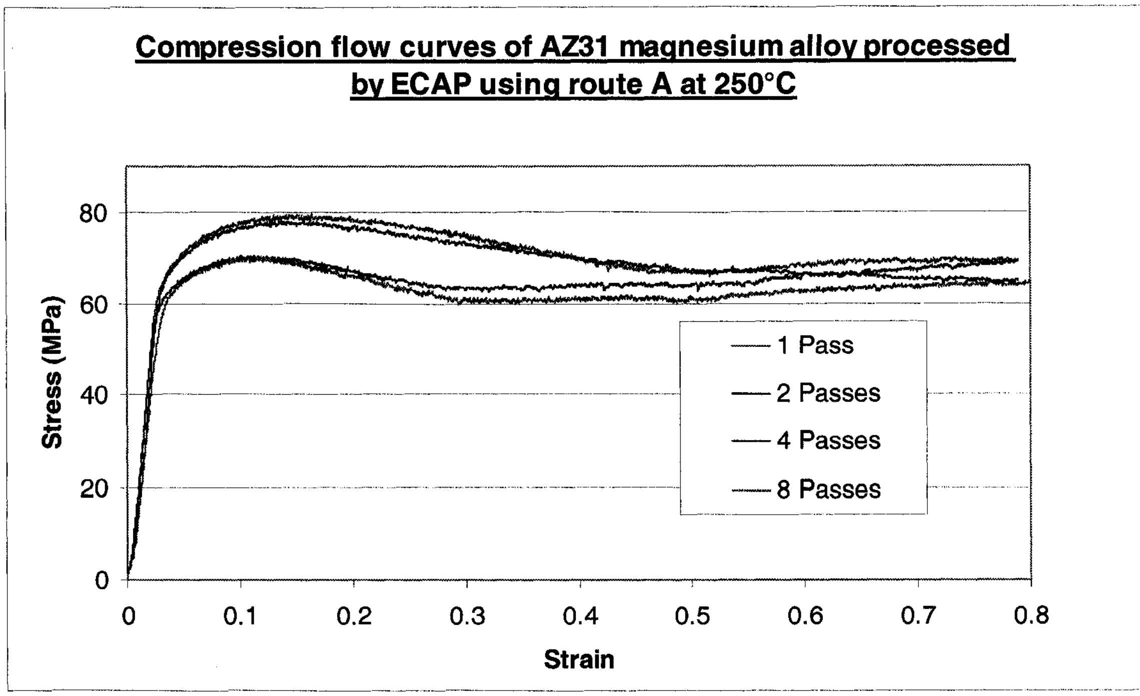
Compression flow curves of AZ31 magnesium alloy processed by ECAP using route A at 250°C
Stress (MPa)
0
20
40
60
80
0
0.1
0.2
0.3
0.4
0.5
0.6
0.7
0.8
Strain
1 Pass
2 Passes
4 Passes
8 Passes

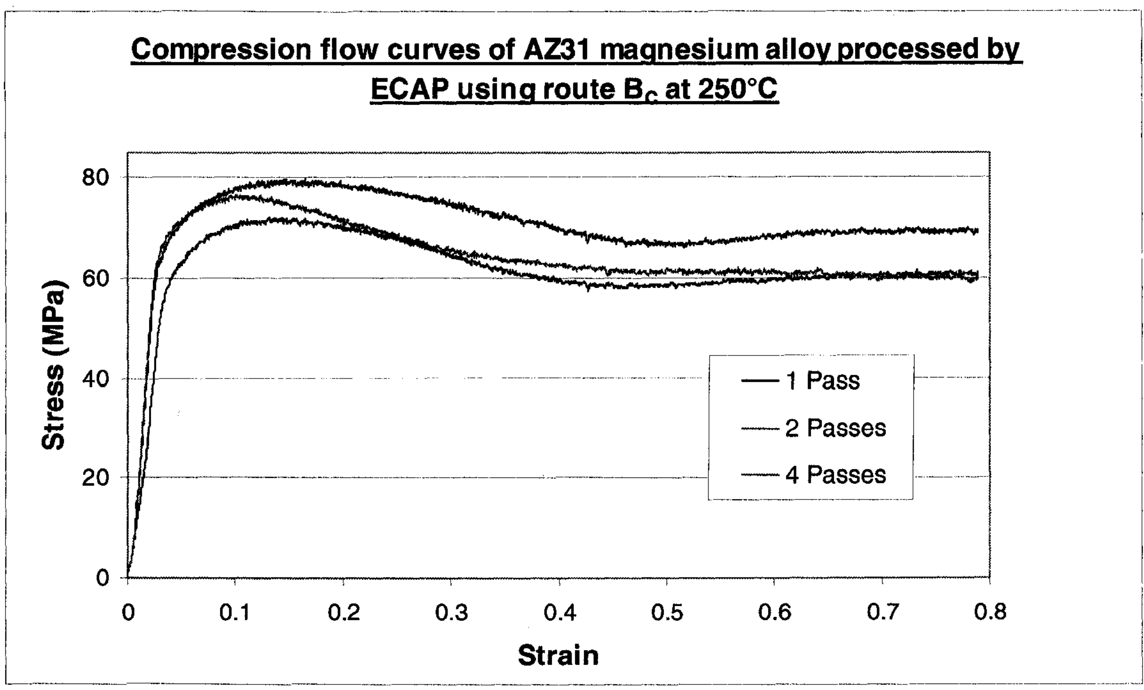
Compression flow curves of AZ31 magnesium alloy processed by ECAP using route B$_C$ at 250°C
Stress (MPa)
0
20
40
60
80
0
0.1
0.2
0.3
0.4
0.5
0.6
0.7
0.8
Strain
1 Pass
2 Passes
4 Passes

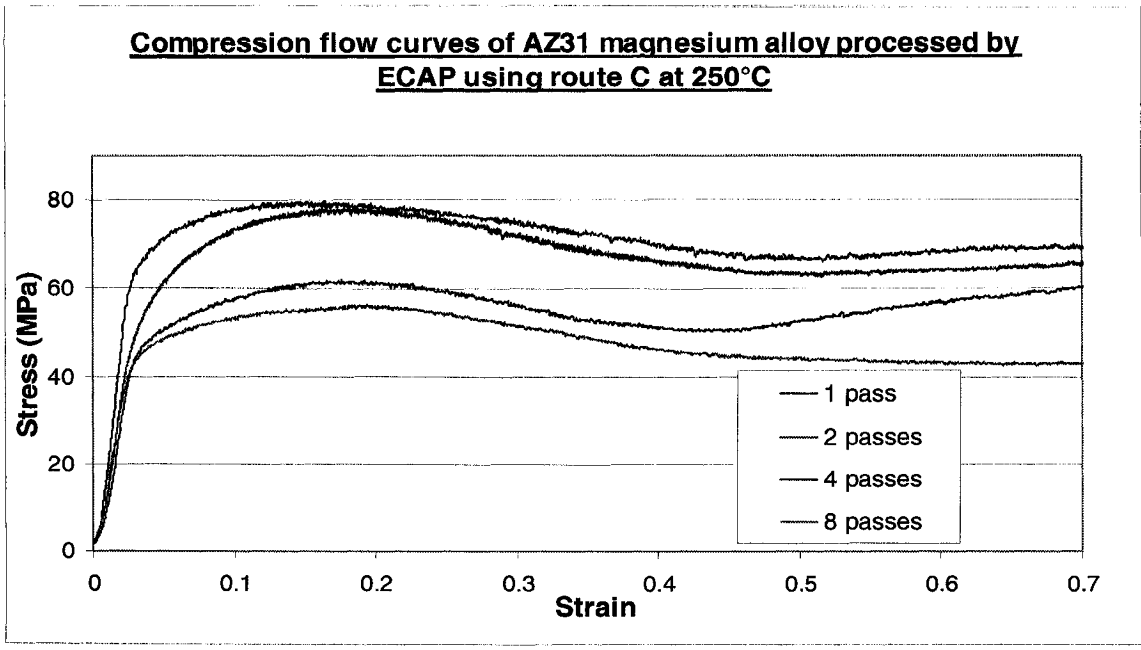

Figure 4.17. Flow curves for samples produced by ECAPing along routes A, B_C and C at 250°C.

Similar remarks apply to the 300°C results, although there is a discrepancy in the route A- 4 pass results, as can be seen in Figure 4.18. This curve exhibits a linear portion following yielding which may indicate the occurrence of extensive twinning.

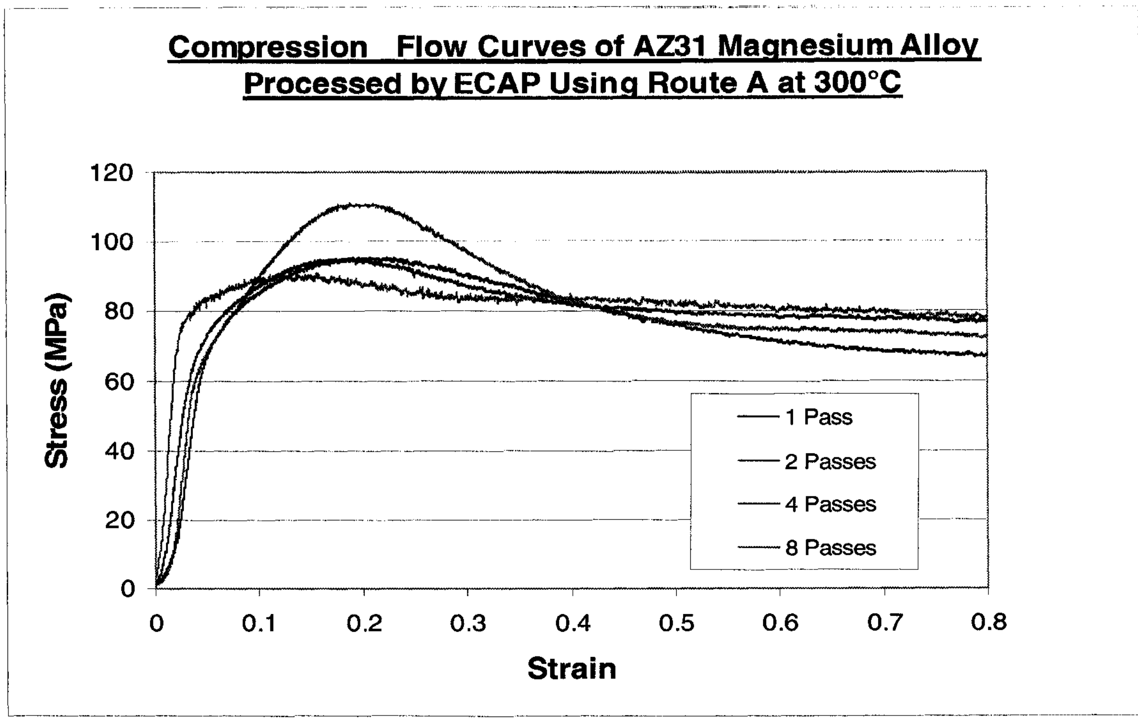
Compression Flow Curves of AZ31 Magnesium Alloy Processed by ECAP Using Route A at 300°C
Stress (MPa)
120
100
80
60
40
20
0
0
0.1
0.2
0.3
0.4
0.5
0.6
0.7
0.8
Strain
1 Pass
2 Passes
4 Passes
8 Passes

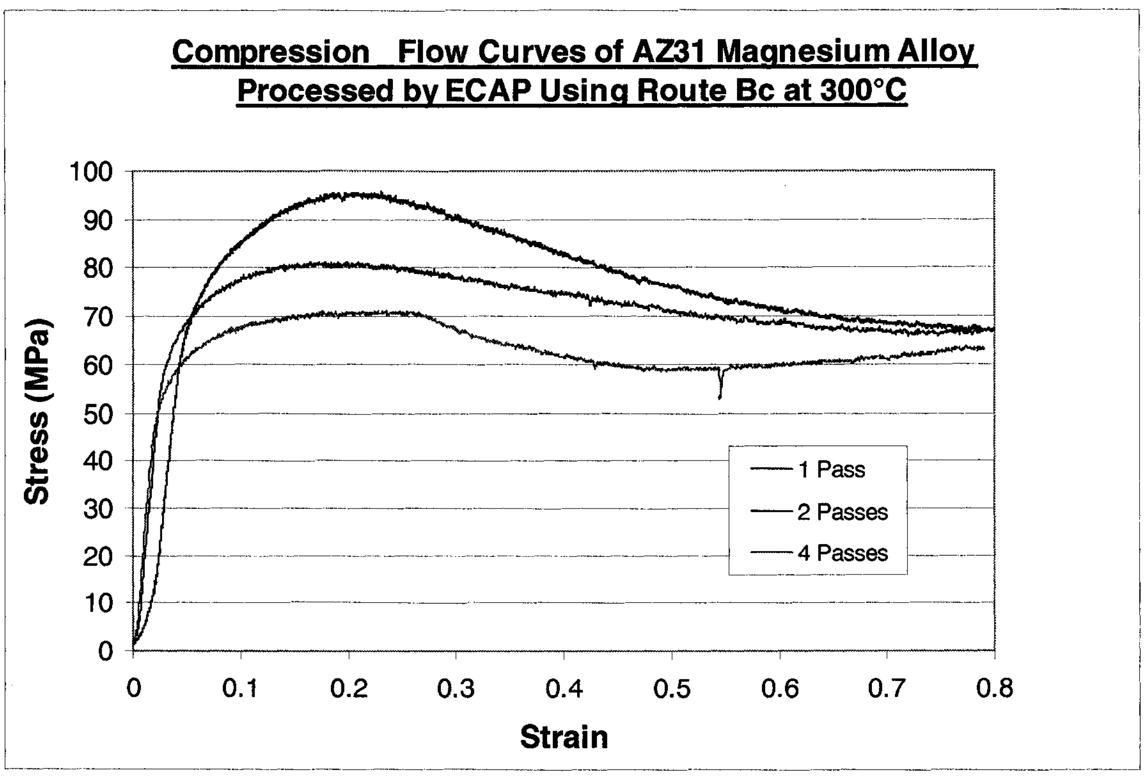
Compression Flow Curves of AZ31 Magnesium Alloy Processed by ECAP Using Route Bc at 300°C
Stress (MPa)
100
90
80
70
60
50
40
30
20
10
0
0
0.1
0.2
0.3
0.4
0.5
0.6
0.7
0.8
Strain
1 Pass
2 Passes
4 Passes

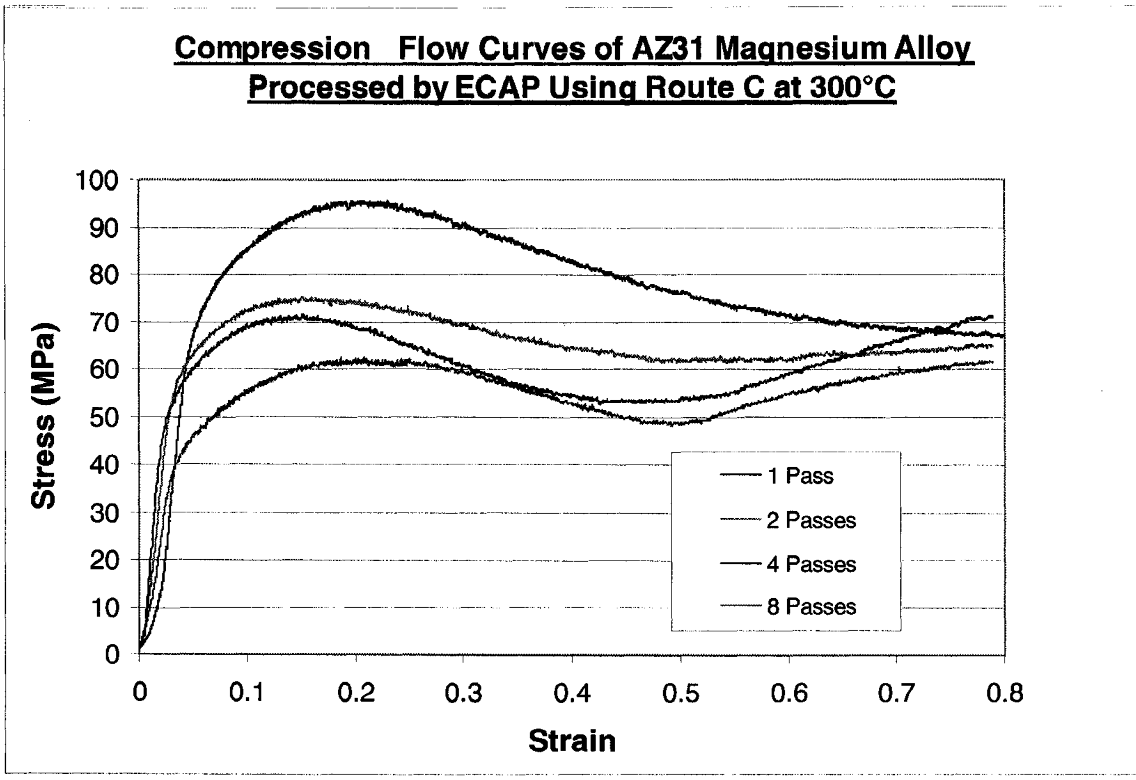

Figure 4.18. Flow curves for samples produced by ECAPing along route A, B_C and C at 300°C.

CHAPTER 5 - DISCUSSION

5.1. Microstructural Analysis

Observing the as-cast ECAPed samples, it is possible to conclude that one pass through the ECAP die is sufficient to break up the cast structure. While one pass is not enough to recrystallize all the grains and large sheared grains remain in the sample, the grain size is refined considerably and precipitates are no longer found at the grain boundaries.

Unfortunately, the high operating temperatures used to compensate for the cast structure caused incipient melting, preventing further experimentation. Using *extruded* material enabled the experiments to be conducted at lower temperatures, inhibiting incipient melting and facilitating successful extrusion.

When the microstructures of extruded one-pass material processed at three temperatures are compared, as presented in Figure 5.1, it is possible to conclude that, at 200°C, the necklaced regions include grains that are much finer than those observed at 250°C. It is possible to clearly distinguish the shearing direction in the grains of the one-pass sample deformed at 250°C while, because of the complete recrystallization taking place at 300°C, it is less evident at the latter temperature.

One ECAP pass at 250°C does not produce enough strain to induce recrystallization in the whole sample. A second pass is necessary to recrystallize the remaining large grains. However, at 300°C, one pass is sufficient to recrystallize all the grains. Further passes simply result in more refinement.

(a)

(b)

(c)

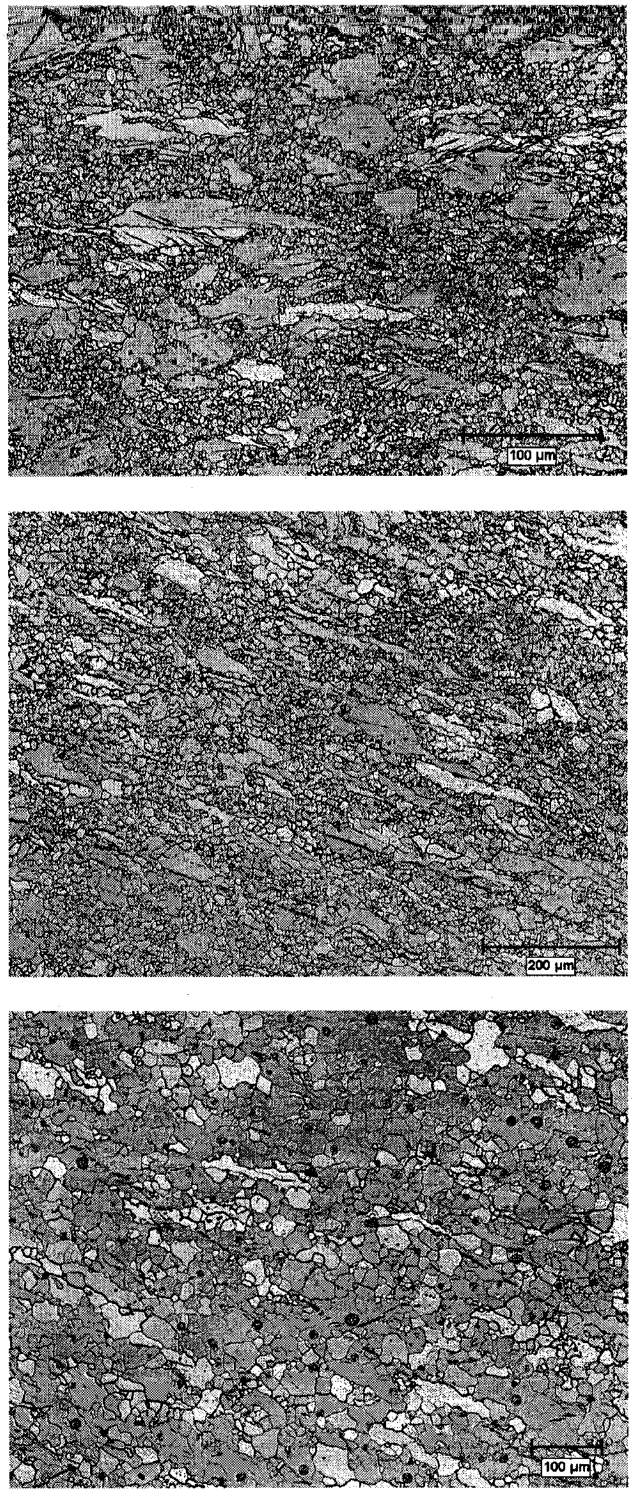

Figure 5.1. Microstructures of extruded 1-pass ECAPed samples deformed at (a) 200°C, 200 x, (b) 250°C, 100 x, and (c) 300°C, 100 x.

It is apparent that increasing the operating temperature results in a net increase in the final grain size. This is caused by the grain growth that occurs following deformation. On average, the sample remains in the die for 15 minutes following each pass. It therefore undergoes an automatic heat treatment after straining. This is unavoidable because of the design of the die. Such a delay provides ample time for the grains to grow significantly before the sample can be quenched and, as the temperature is increased, so does the grain growth rate, resulting in larger grains. Increasing the number of passes results in a finer grain size as severe shear is applied over and over; nevertheless grain growth affects the final grain size no matter what the route. This has been shown for AZ61 by Kim *et al.* [22]-[25].

In the present work, when route B_C was followed, it was evident that there was an increase in grain refinement in going from the two-pass to the four-pass material. This difference in grain size was more pronounced than for routes A and C, where the grain refinement seemed to stop after the second pass at 250°C. The microstructure seems appreciably finer too considering that only four passes were achieved successfully for that route. This appears to be because shearing is applied to all three planes under these conditions, as discussed above.

5.2. Mechanical Testing by Compression

Looking at the results from the compression tests, it is possible to see that using an ECAP path with shearing in more directions, such as route C, results in the width of the flow curve being broader than that corresponding to route A, as seen in Figure 5.2a. The use of route C resulted in slightly finer grains. When these samples were subjected to compression at 200°C, grain boundary sliding occurred, reducing the strength in compression to less than that associated with the coarser microstructure. As the temperature of ECAPing was increased, the grains become coarser, the strength in compression increased, the rate of work hardening was positive over a shorter strain interval (Figure 5.2), and therefore the ductility expected in tension decreased.

Eventually the true stress increased, due to the change in cross-section, becoming greater than the load-carrying ability of the metal due to strain hardening. This is what finally leads to failure in tension.

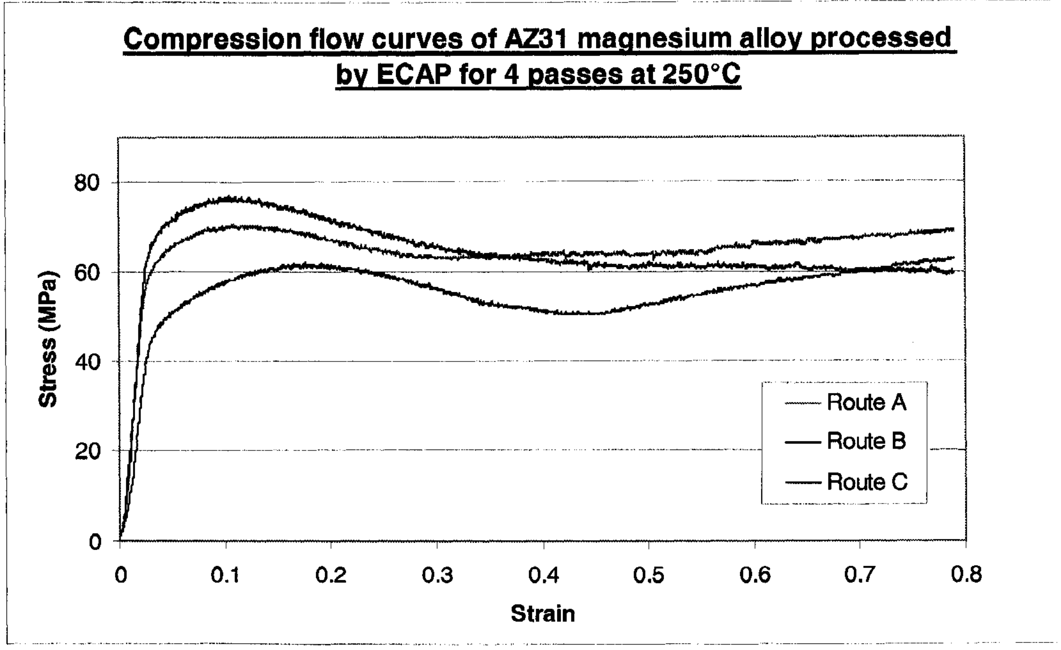

(a)

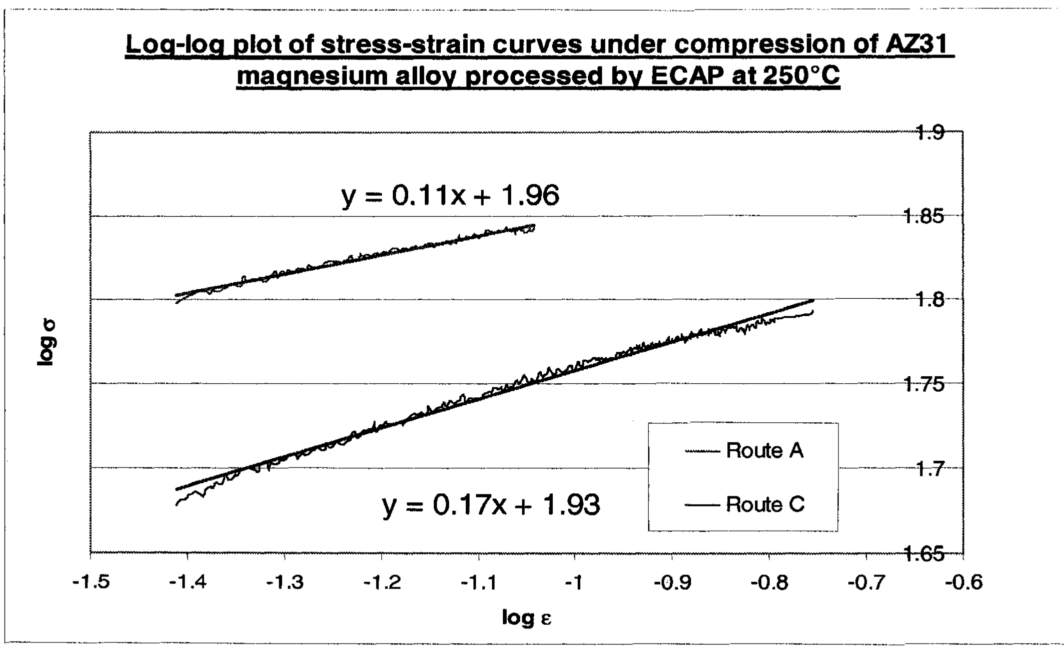

(b)

Figure 5.2. (a) Compression flow curves of AZ31 alloy processed by ECAP using different paths for 4 passes at 250°C and (b) log-log plot for routes A and C.

The compression tests completed at 200°C are in the hot working temperature range ($T_{homologous} = T_{compression}/T_{mp} = 473K/973K = 0.51 > 0.4$) and, therefore, grain boundary sliding is expected to be the controlling deformation mode in the finer grained materials. Nevertheless, under conditions similar to those of the present experiments, Agnew *et al.* [27],[30] and Kim *et al.* [25] found that texture played a greater role than it did in this investigation.

Observing the compression flow curves determined on the 1-pass material at the three temperatures, it is evident that the strength (UTS and YS) increases with the temperature of ECAP processing, see Figure 5.3. Another alternative is that a finer grain size promotes the nucleation of dynamic recrystallization. As the latter, like grain boundary sliding and superplasticity, is a softening mechanism, further experiments would have to be carried out to distinguish between these two effects. This is clearly a *grain size* rather than a texture effect.[1]

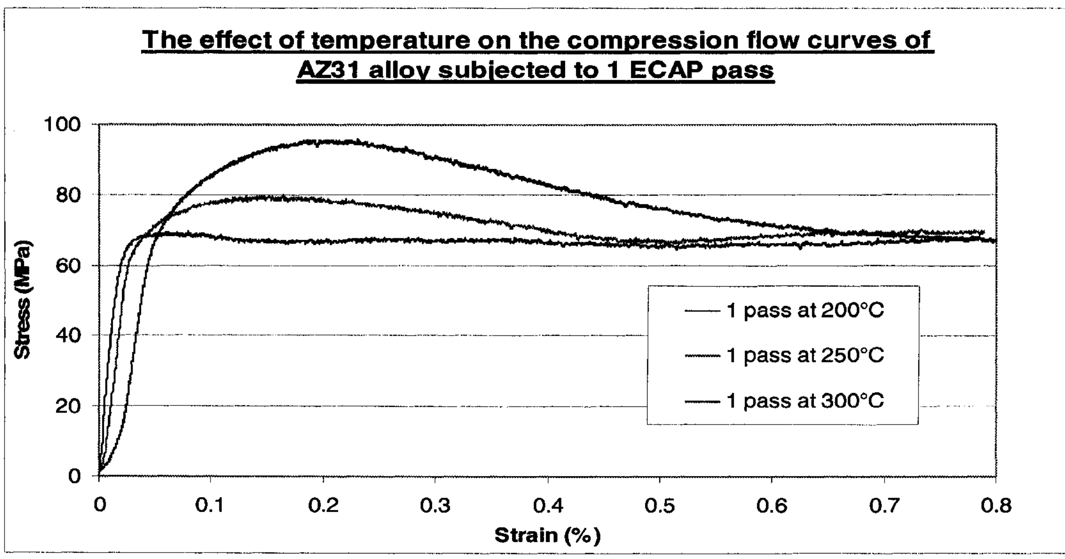

Figure 5.3. Compression flow curves determined at 200°C on material processed through ECAP for 1 pass at various temperatures.

[1] Note that the 300°C texture contains a weak component of the basal poles oriented along the compression axis (see Figure 4.13). This component also makes a small contribution to strengthening at this temperature.

5.3. Texture Analysis

The initial texture of conventionally extruded magnesium is that of the basal poles being perpendicular to the extrusion direction, as illustrated in Figure 5.4. After one ECAP pass at 200°C, a preferred orientation with the basal planes inclined 45° to the ECAP axis is developed. The same can be observed at 250°C (Figure 5.5 (a)), but at 300°C (Figure 5.5 (b)), there is a change in the texture of the material as a result of dynamic recrystallization. This is supported by the microstructure in Figure 5.1 (c), where it is evident that the 300°C material is fully recrystallized.

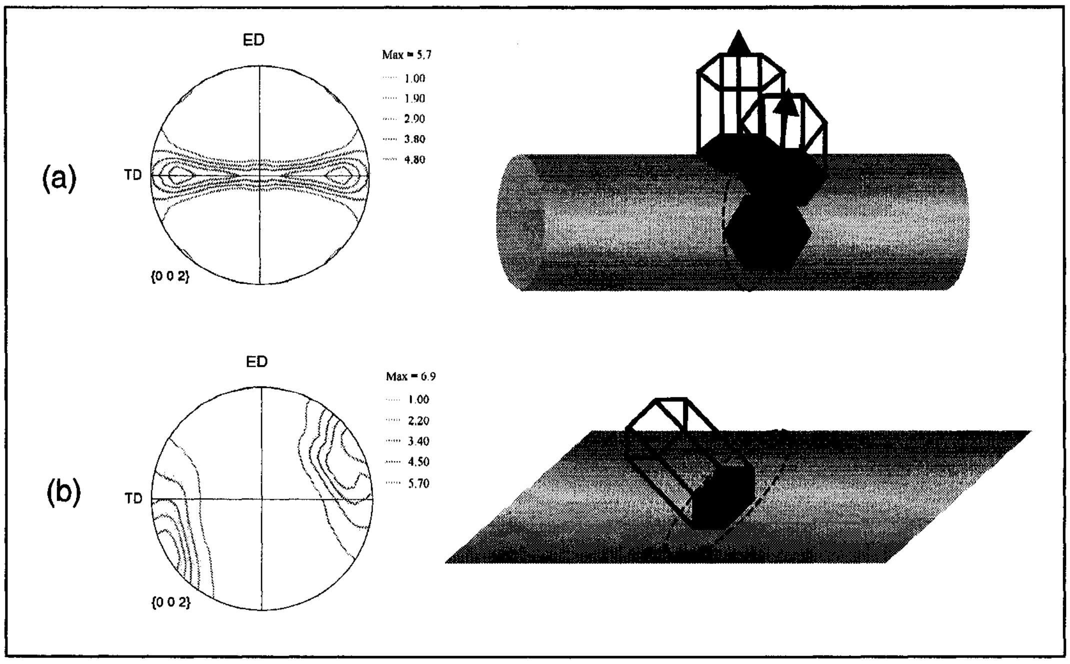

Figure 5.4. Illustration of the orientations of the basal poles and planes according to the texture measurements for the (a) as-extruded annealed material and (b) after 1 ECAP pass at 200°C.

For route A, it seems that, as more and more passes are applied, the original fiber texture tends towards a rolling texture, as seen in Figure 5.6. This could be due to the recrystallized volume fraction increasing per pass, as discussed previously. But it could also have to do with the shearing of the sample.

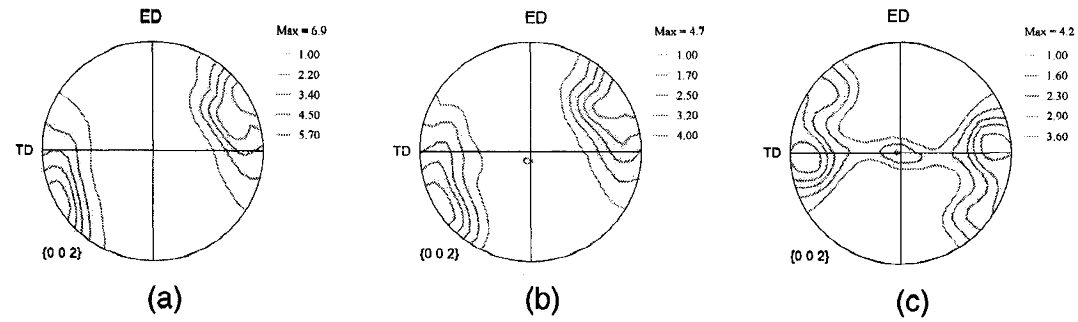

Figure 5.5. Basal pole figures for material after 1 pass at (a) 200°C, (b) 250°C, and (c) 300°C.

Examination of a square element in the material undergoing the forming operation enables us to understand the relationship between shearing and texture, as seen in the following figure.

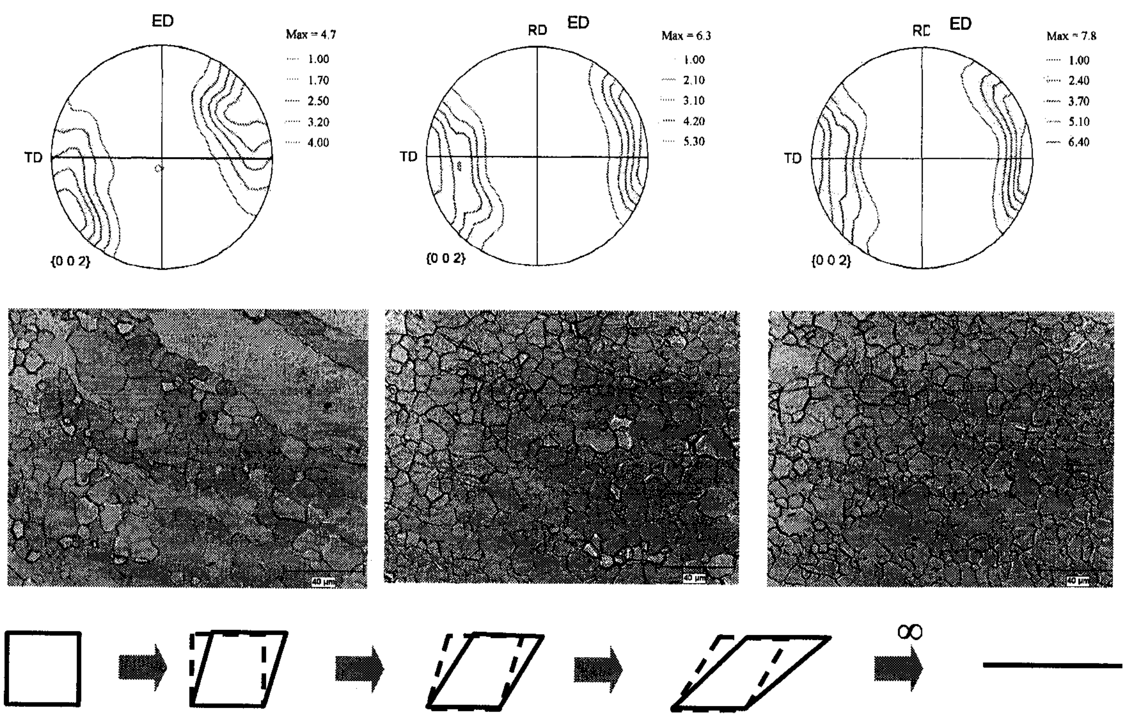

Figure 5.6. Illustration of the effect of accumulated shear within the sample as the number of passes is increased. The basal poles and microstructures corresponding to samples processed along route A at 250°C are shown for 1, 2 and 4 passes.

For route C, on the other hand, repeating the ECAP procedure does not change the texture, which retains its 45° preferential orientation as seen in Figure 5.7. Once again, examining the shearing properties of the material, this means that one pass of ECAP is sufficient to return the material to its previous preferred orientation, regardless of the initial orientation. Whether the initial texture is as-extruded or a preferred orientation that has been turned by 180°, the result of each pass is the same preferred orientation. Of course, this does not apply if dynamic recrystallization is initiated.

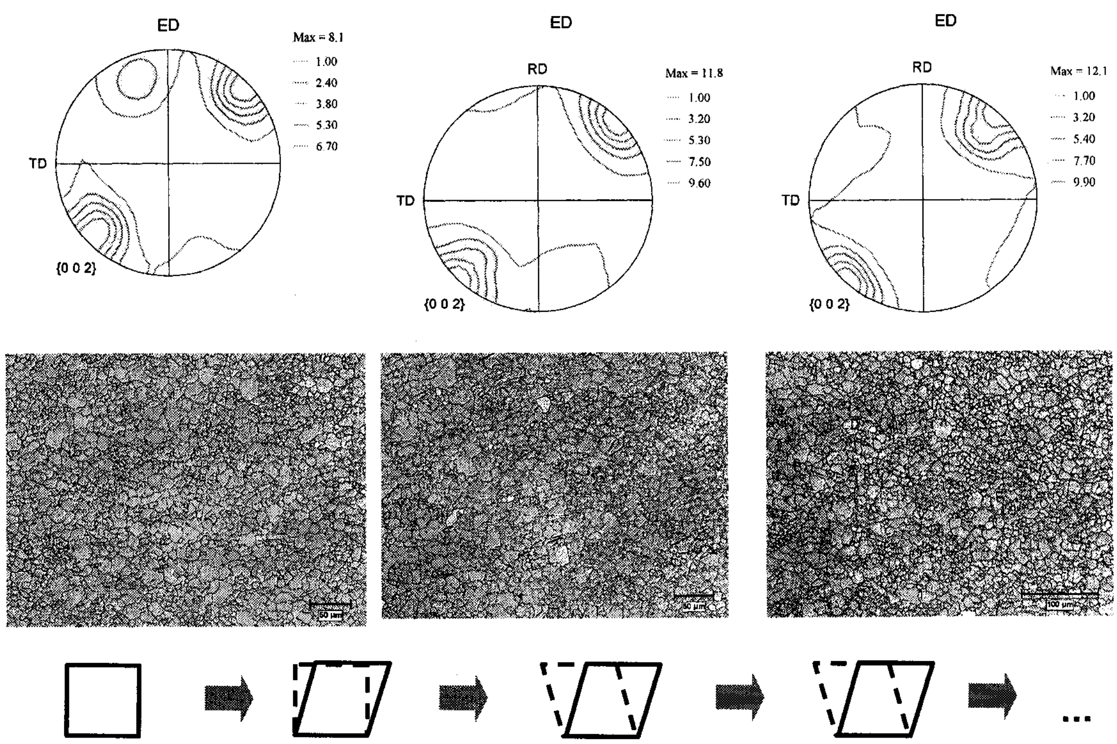

Figure 5.7. Illustration of the effect of accumulated shear within the sample as the number of passes is increased. The basal poles and microstructures corresponding to samples processed along route C at 250°C are shown for 1, 2 and 4 passes.

5.4. Shear Instabilities

(a)
(b)
(c)

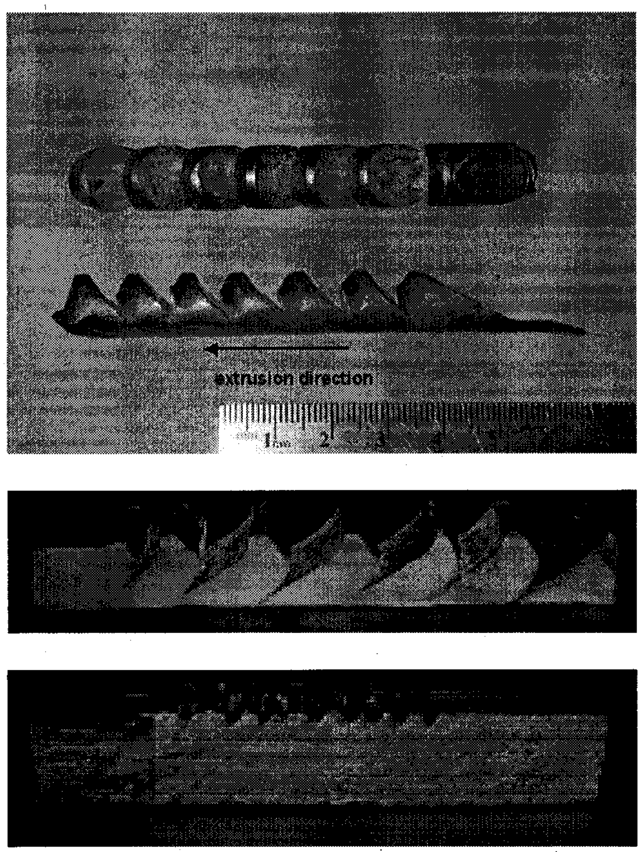

Figure 5.8. Shear failures exhibited by an AZ31 sample processed by ECAP (a) at 200°C (present work - no back pressure), and (b) at 200°C without back pressure and (c) 175°C with back pressure (Agnew *et al.* [30]).

We turn now to the catastrophic shear failures that are illustrated in Figure 5.8. Figure 5.8 (a) is from the present work, whereas Figure 5.8 (b) is reproduced from the results reported by Agnew *et al.* [30]. The latter authors did not, however, provide an explanation of this phenomenon. Note that both the experiments of Figure 5.8 (a) and Figure 5.8 (b) were carried out at 200°C, at which the flow stress of magnesium is relatively high.

A possible interpretation of this phenomenon will now be introduced. It should be noted that the failures seen in these figures are of the nature of shear instabilities. Such instabilities arise when deformation is heavily concentrated on a single shear plane and the deformation heating produced on this plane does not have sufficient time to diffuse away. This has the potential to lead to a vicious circle leading to this shear instability.

A way of assessing the likelihood of shear instability is to consider the ratio of the work done (energy stored and heat produced) to the capacity of the material to absorb the heat and for it to diffuse away. Neglecting energy storage, the rate of heat production is given by the product of σ and $\dot{\varepsilon}$, which defines the work done per unit volume per unit time. The rate at which heat is conducted away from the shear plane (per unit area) is given by the product $k \cdot \Delta T/\Delta x$, where k is the coefficient of thermal conductivity in W/m·K and $\Delta T/\Delta x$ is the temperature gradient. The heat capacity is in turn given by the product $\rho \cdot c_p$ (ρ: specific gravity, c_p: heat capacity per unit volume).
This leads to a parameter that indicates the likelihood of shear localization:

$$\frac{\sigma \cdot \dot{\varepsilon} \cdot \Delta x}{k \cdot \rho \cdot c_p \cdot A \cdot \Delta T}$$

High values of k, c_p, and ρ, will *reduce* the above parameter and the likelihood of localization as they represent the capacity to absorb or dissipate heat.

The units of the above expression are K/J. This represents a temperature rise of K degrees per Joule of work done and hence the higher this value, the more likely instabilities will occur during forming.

When the strain rate ($\dot{\varepsilon}$) is *high*, there is little time for the heat to diffuse. Similarly, high (mean) flow stress (σ) means the work done is high and the heat produced significant. The latter can be either released or accumulated. For simplicity, all the metals listed in the table below are assumed to have the same (constant) flow stress at the forming temperature. It should also be noted that the cross-section is taken as a unit area and $\Delta T/\Delta x$ is a unit temperature gradient. The determining value is then:

$$\frac{1}{k \cdot \rho \cdot c_p}$$

We can see from Table 5.1 that AZ31 has the highest value (except for Ti and Zr). This means that it is more susceptible to shear localization than most other metals, as can be observed above in Figure 5.8.

It is evident that the most commonly used metal, iron, with its body-centered cubic crystal structure, has a lower value of the parameter (than AZ31) and is therefore more formable. This can explain its common commercial use for various applications. Note that the face-centered cubic metals, such as copper, gold and silver, have still lower values of the parameter than iron and values that are well below those of the hexagonal metals. This is consistent with their high formabilities.

Table 5.1. Element and alloy parameters defining likelihood of shear instability

Crystal Structure	Element	Thermal Conductivity (W/mK), k	Density (Mg/m3), ρ	Specific Heat at 25°C (J/kgK), c_P	$k \cdot \rho \cdot c_P$	$1/k \cdot \rho \cdot c_P$ ($\times 10^{-9}$)
HCP	AZ31	96	1.77	1050	1.78E+08	5.60
	Mg	418	1.738	1025	7.45E+08	1.34
	Ti	21.6	4.507	522.3	5.08E+07	19.67
	Zn	113	7.133	382	3.08E+08	3.25
	Zr	21.1	6.505	200	2.75E+07	36.43
	Cd	98	8.642	230	1.95E+08	5.13
	Co	69.04	8.832	414	2.52E+08	3.96
FCC	Al	247	2.6989	900	6.00E+08	1.67
	Ag	428	10.49	235	1.06E+09	0.95
	Au	317.9	19.302	128	7.85E+08	1.27
	Cu	398	8.93	386	1.37E+09	0.73
	Ni	82.9	8.902	471	3.48E+08	2.88
BCC	Fe	80.4	7.87	447.3	2.83E+08	3.53

CHAPTER 6 - CONCLUSIONS

1) When low operating temperatures were employed to process some as-cast AZ31 by means of ECAP, shear instabilities were produced. This is because the rate of doing work was relatively high; the work was then converted into heat. Localized failure occurred as the high heat output caused melting once the work done was accumulated for a sufficient period of time.

2) ECAP is an effective method of grain refinement, which enhances the ductility. It is apparent that increasing the operating temperature increases the final grain size as a result of grain growth. Conversely increasing the number of passes results in a finer grain size because of the accumulation of shear.

3) The mechanical properties indicate that using a path with shearing in more than one direction, such as route C, results in a broader flow curve than for route A. This appears to be associated with the finer grain size produced by this means as well as with a higher work hardening rate.

4) Increasing the temperature of ECAP results in coarser grains, which in turn yield higher strengths under compression at 200°C. This was because there was less grain boundary sliding. The higher flow stresses of the materials containing the coarser microstructures can be expected to lead to lower ductilities. This is clearly a grain size rather than a texture effect.

5) The effect of grain refinement is greater than that of texture. As the temperature of ECAP'ing is increased, the strength of the resulting product increases and the

ductility decreases. This appears to be due to the coarser grain size of the 300°C product and indicates that the effect of grain refinement is greater than that of texture. This can be interpreted as indicating that grain boundary sliding is important in fine-grained magnesium alloys, reducing the strength (or resistance to flow) of the material. Conversely, grain boundary sliding does not play a significant role in the deformation of the coarse-grained alloys. These consequently have higher flow stresses.

6) Zirconium and titanium are the two metals that are the most susceptible to shear localization (a reason why titanium alloys are often forged at very low strain rates using isothermal forging). Nevertheless, the susceptibility of AZ31 (and other magnesium alloys) to flow localization is greater that that of the other metals used commercially.

REFERENCES

[1] Mordike BL, Ebert T. Magnesium: Properties — applications — potential, Mater Sci. Eng. A Vol. 302 (2001) p. 37.

[2] Horita Z, Fujinami T, Langdon TG. The potential for scaling ECAP: effect of sample size on grain refinement and mechanical properties, Mater. Sci. Eng. A Vol. 318 (2001) p. 34.

[3] Iwahashi Y, Furukawa M, Horita Z, Nemoto M, and Langdon TG. Microstructural characteristics of ultrafine-grained aluminum produced using equal angular pressing, Metall. Mat. Trans. Vol.A29 (1998) p. 2245.

[4] Smith, William F., Structure and Properties of Engineering Alloys, 2nd edition, McGraw-Hill Series in Materials Science and Engineering, 1993.

[5] Barnett MR. Influence of deformation conditions and texture on the high temperature flow stress of magnesium AZ31, Jour. Light Met. Vol. 1 (2001) p. 167.

[6] Staroselsky A and Anand L. A constitutive model for hcp materials deforming by slip and twinning: application to magnesium alloy AZ31B, Internat. Jour. Plast. Vol. 19 (2003) p. 1843.

[7] Ravi Kumar NV, Blandin JJ, Desrayaud C, Montheillet F, and Suery M. Grain refinement in AZ91 magnesium alloy during thermomechanical processing, Mat. & Eng. Vol. A359 (2003) p. 150.

[8] Barnett MR. Hot working magnesium AZ31.

[9] Wonsiewicz BC, Backofen WA. Trans. Metall. Soc. AIME (1967) Vol. 239 p. 1422.

[10] Hartt WH, Reed-Hill RE. Trans. Metall soc. AIME Vol. 242 (1968) p. 1121.

[11] Koike J. Metall. Mater. Trans. A Vol. 36 (2005) p. 1689.

[12] Nave MD, Barnett MR. Scripta Mater. Vol 51 (2004) p. 881.

[13] Jiang L, Jonas JJ, Luo AA, Sachdev A, Godet S. Twinning-induced softening in polycrystalline AZ30 Mg alloy at moderate temperatures, Scripta Mater. Vol 54 (2006) p. 771.

[14] Kocks UF, Tome CN, Wenk HR. Texture and Anisotropy Preferred Orientations in Polycrystals and their Effect on Materials Properties, Cambridge University Press, 1998, pp. 203-207.

[15] Mukai T, Mohri T, Mabuchi M, and Nakamara M. Experimental study of a structural magnesium alloy with high absorption energy under dynamic loading, Scripta Mat Vol. 39 (1998) p. 1249.

[16] Mukai T, Yamanoi M, Watanabe H, and Higashi K. Ductility enhancement in AZ31 magnesium alloy by controlling its grain structure, Scripta Mat. Vol.45 (2001) p. 89.

[17] Valiev RZ, Islamgaliev RK, Alexandrov IV. Bulk nanostructured materials from severe plastic deformation, Prog. Mater. Sci. Vol. 45 (2000) p. 103.

[18] Furukawa M, Horita Z, Nemoto M, Langdon TG. The use of severe plastic deformation for microstructural control, Mater. Sci. Eng. A Vol. 324 (2002) p. 82.

[19] Berbon PB, Tsenev NK, Valiev RZ, Furukawa M, Horita Z, Nemoto M, and Langdon TG. Fabrication of bulk ultrafine-grained materials though intense plastic straining, Metall. Mat. Trans. Vol. 29A (1998) p. 2237.

[20] Iwahashi Y, Horita Z, Nemoto M, and Langdon TG. The process of grain refinement in equal-channel angular pressing, 1998 Acta Mat. Vol. 49 No.9 p. 3317.

[21] Nakashima K, Horita Z, Nemoto M, and Langdon TG. Influence of channel angle on the development of ultrafine grainds in equal-channel angular pressing, 1998 Acta Mat. Vol. 46 No.5 p. 1589.

[22] Kim WJ, Hong SI, Kim YS, Min SH, Jeong HT, and Lee JD. Texture development and its effect on mechanical properties of an AZ61Mg alloy fabricated by equal channel angular pressing, Acta Mat. Vol. 51 (1998) p. 3293.

[23] Furukawa M, Ma Y, Horita Z, Nemoto M, Valiev RZ, and Langdon TG. Microstructural characteristics and superplastic ductility in a Zn-22% Al alloy with submicrometer grain size, Mater. Sci. Eng. Vol. A241 (1998) p. 122.

[24] Furukawa M, Iwahashi Y, Horita Z, Nemoto M, and Langdon TG. The shearing characteristics associated with equal-channel angular pressing, Mat. Sci. Eng. Vol. A257 (1998) p. 328.

[25] Kim WJ, An CW, Kim YS, and Hong SI. Mechanical properties and microstructures of an AZ61 Mg Alloy produced by equal channel angular pressing, Scripta Mat. Vol. 47 (2002) p. 39.

[26] Yamachita A, Horita Z, and Langdon TG. Improving the mechanical properties of magnesium and magnesium alloy through severe plastic deformation, Mat. Sci. and Eng. Vol. A300 (2001) p. 142.

[27] Agnew SR, Horton JA, Lillo TM, and Brown DW. Enhanced ductility in strongly textured magnesium produced by equal channel angular processing, Scripta Mat. Vol. 50 (2004) p. 377.

[28] Koike J, Kobayashi T, Mukai T, Watanabe H, Suzuki M, Maruyama K, and Higashi K. The activity of non-basal slip systems and dynamic recovery at room temperature in fine-grained AZ31B magnesium alloys, Acta Mat. Vol. 51 (2003) p. 2055.

[29] Eddahbi M, del Valle JA, Pérez-Prado MT, Ruano OA. Comparison of the Microstructure and thermal stability of an AZ31 alloy processed by ECAP and large strain hot rolling, Mater. Sci. Eng. A Vol. 410-411 (2005) p. 308.

[30] Agnew SR, Mehrotra O, Lillo TM, Stoica GM, Liaw PK. Texture evolution of five wrought magnesium alloys during route A equal channel angular extrusion: Experiments and simulations, Acta Mater. Vol. 53 (2005) p. 3135.

[31] Agnew SR, Mehrotra P, Lillo TM, Stoica GM, Liaw PK. Crystallographic texture evolution of three wrought magnesium alloys during equal channel angular extrusion, Mater. Sci. & Eng. A Vol. 408 (2005) p. 72.

[32] R.D. Field, K.T. Hartwig, C.T. Necker, J.F. Bingert, S.R. Agnew, Metall. Mater. Trans. 23A (2002) p. 965.

[33] Bowen JR, A. Gholinia A, S. M. Roberts SM, Prangnell PB. Analysis of the billet deformation behaviour in equal channel angular extrusion, Mater Sci. Eng. A Vol. 287 (2000) p. 87.

[34] Beyerlein IJ, Tomé CN. Analytical modeling of material flow in equal channel angular extrusion (ECAE), Mater. Sci. Eng. A Vol. 380 (2004) p. 171.

[35] Wu Y, Baker I. An experimental study of equal channel angular extrusion, Scripta Mater. Vol. 37 (1997) p. 437.

[36] Pilling J and Ridley N. Superplasticity in Crystalline Solids, The Institute of Metals, Vol. 31 (1989).

[37] Langdon TG. The mechanical properties of superplastic materials, Metall. Trans. Vol. 13A, May 1982, p. 689.

[38] Galiev A and Kaibyshev R. Microstructural evolution in ZK60 magnesium alloy during severe plastic deformation, Mat. Trans. Vol. 42, No. 7 (2001) p. 1190.

[39] Tan JC and Tan MJ. Superplasticity and grain boundary sliding characteristics in two stage deformation of Mg-3Al-1Zn alloy sheet, Mat. Sci. Eng Vol. A339 (2003) p. 81.

[40] Tsutsui H, Watanabe H, Mukai T, Kohzu M, Tanabe S, and Higashi K. Superplastic deformation behavior in commercial magnesium Alloy AZ61, Mat. Trans. Vol. 40, No. 9 (1999) p. 931.

[41] Mabuchi M., Iwasaki H, Yanase K, and Higashi K. Low temperature superplasticiy in an AZ91 magnesium alloy processed by ECAE, Scripta Mat. Vol. 36-6 (1997) p. 681.

[42] Mohri T and Mabuchi M. Microstructural evolution and superplasticity of rolled Mg-9Al-1Zn, Mat. Sci. Eng Vol. A290 (2000) p. 139.

[43] Wei YH, Wang QD, Zhu YP, Zhou HT, Ding WJ, Chino Y, and Mabuchi M. Superplasticity and grain boundary sliding in rolled AZ91 magnesium alloy at high strain rates, Mat. Sci. Eng. Vol. A360 (2003) p. 107.

[44] Matsubara K, Miyahara Y, Horita Z, and Langdon TG. Developing superplasticity in a magnesium alloy through a combination of extrusion and ECAP, Acta Mat. Vol.51 (2001) p. 3073.

APPENDIX A

MACHINING OF EXTRUSION SAMPLES FROM AS-CAST INGOT

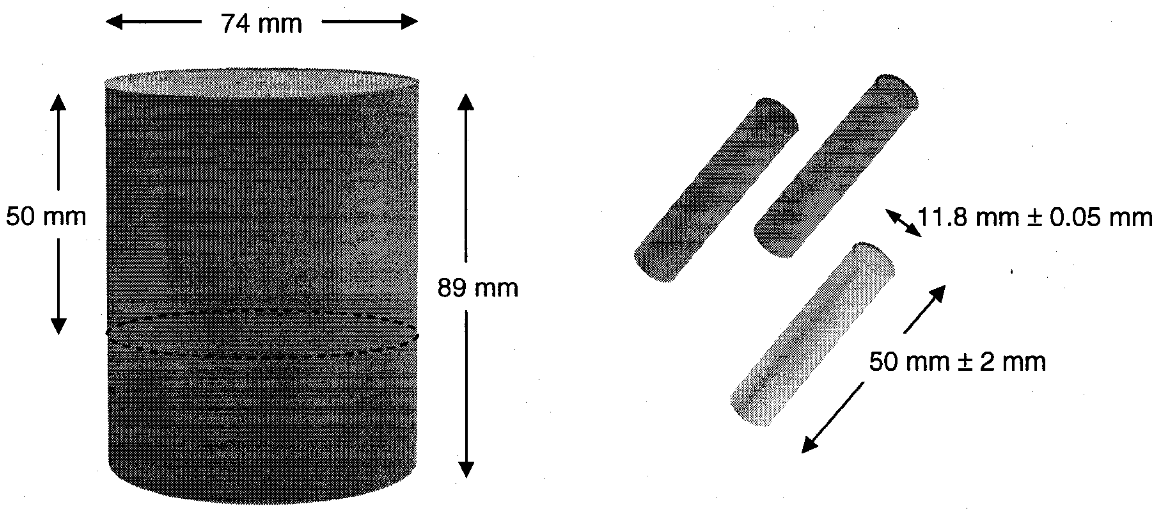

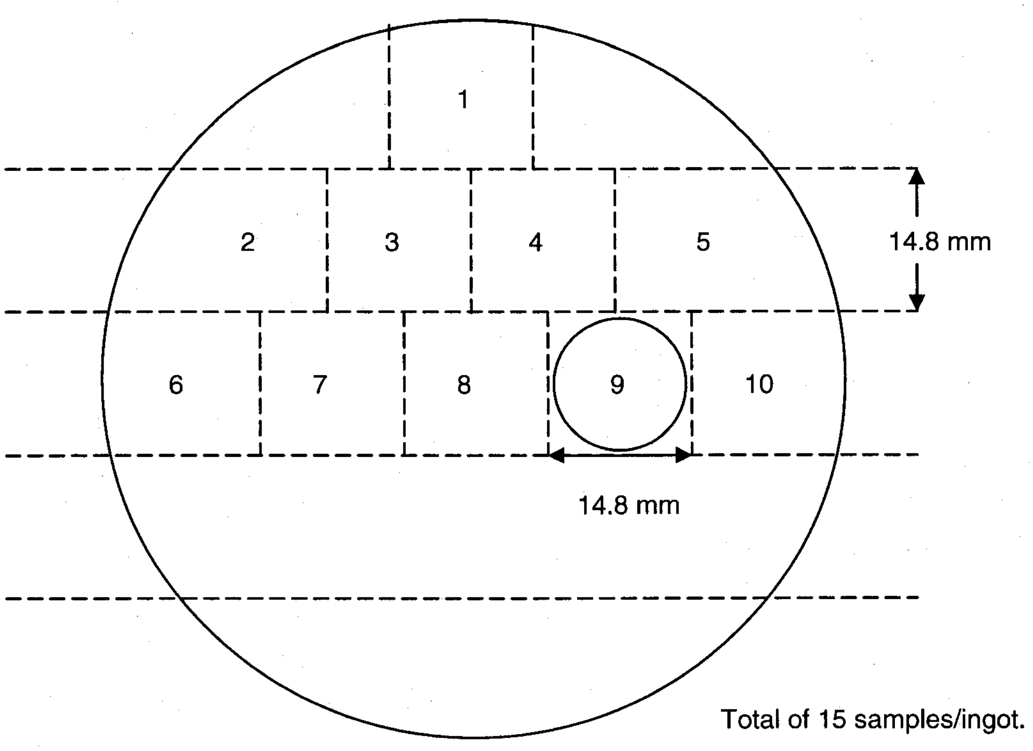

APPENDIX B

RESULTS OF TEXTURE ANALYSIS BY X-RAY DIFFRACTION

Sample Information

As-extruded and annealed at 350°C for 1 hour

Pole Figures

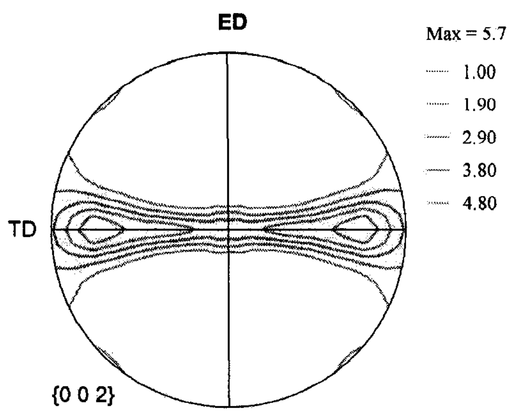

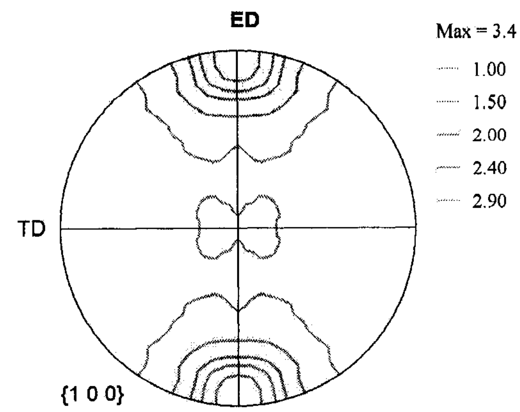

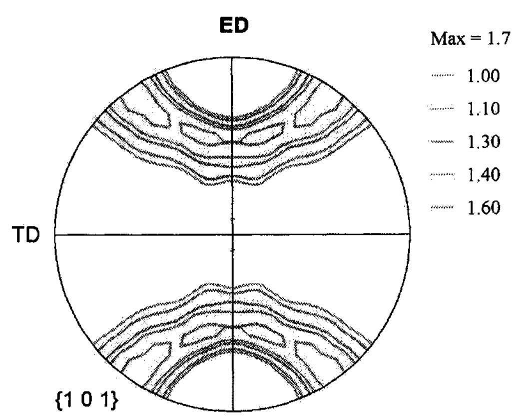

Inverse Pole Figures

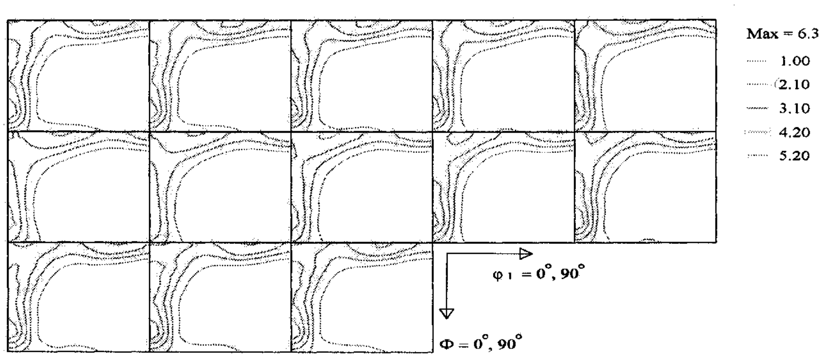

APPENDIX B (cont'd)

Sample Information

Total number of pass(es): 1
Temperature of ECAP: 200°C

Pole Figures

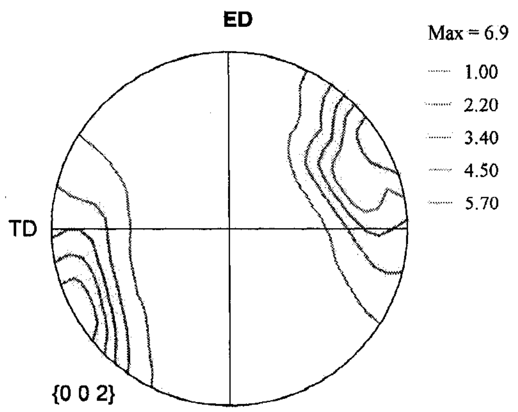

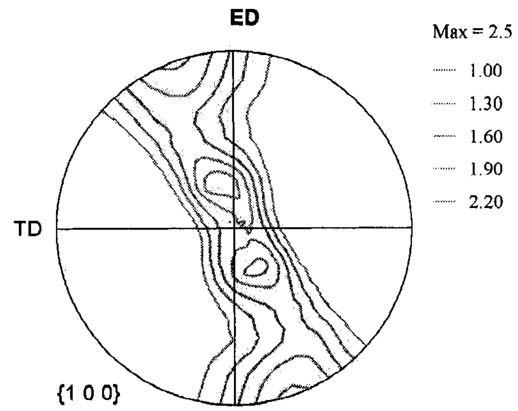

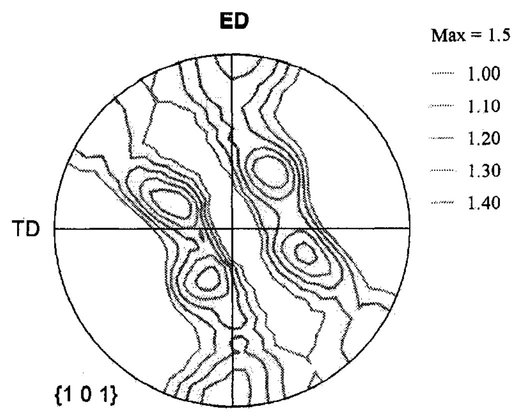

Inverse Pole Figures

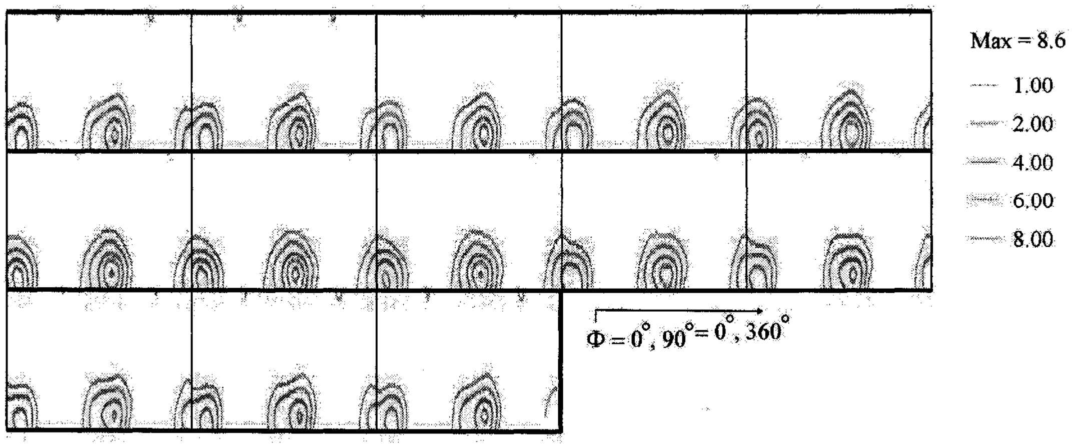

APPENDIX B (cont'd)

Sample Information

Total number of pass(es): 1
Temperature of ECAP: 250°C

Pole Figures

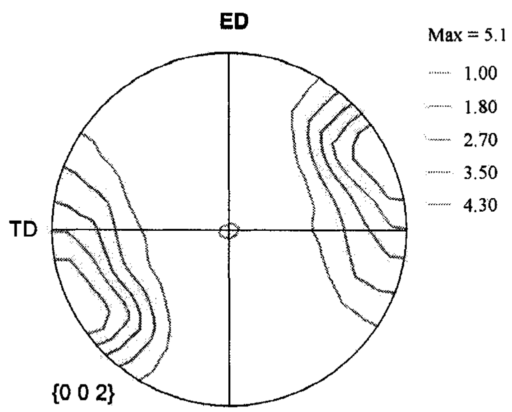

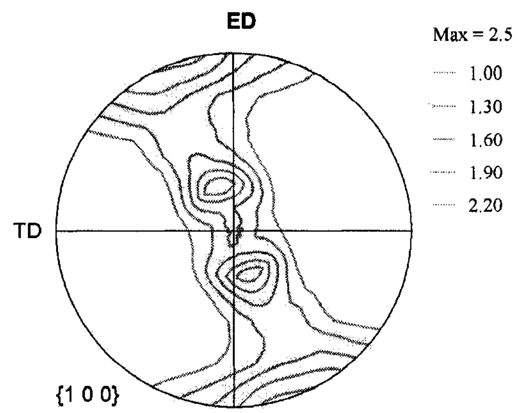

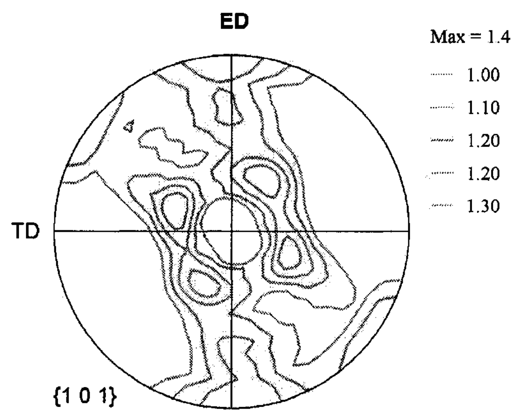

Inverse Pole Figures

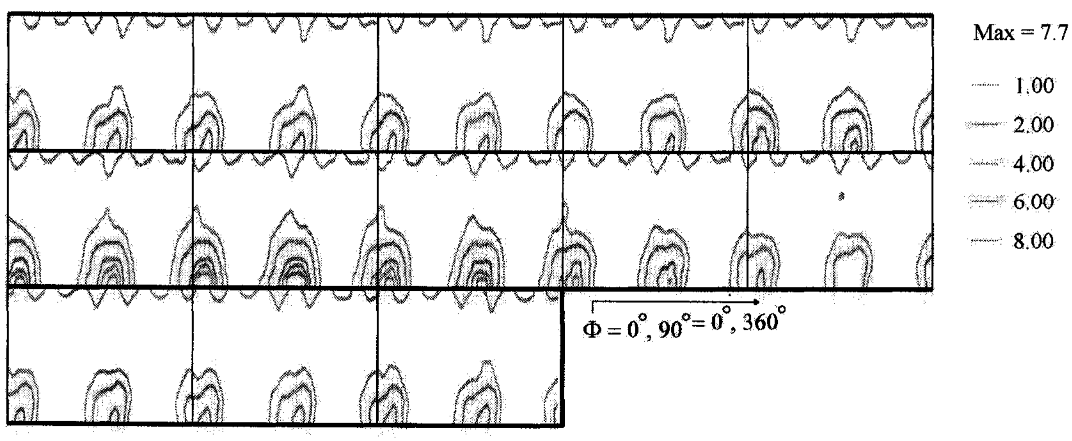

APPENDIX B (cont'd)

Sample Information

Route: A (0° rotation)
Total number of pass(es): 2
Temperature of ECAP: 250°C

Pole Figures

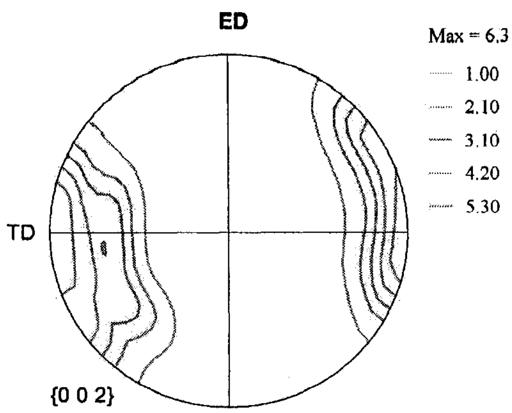

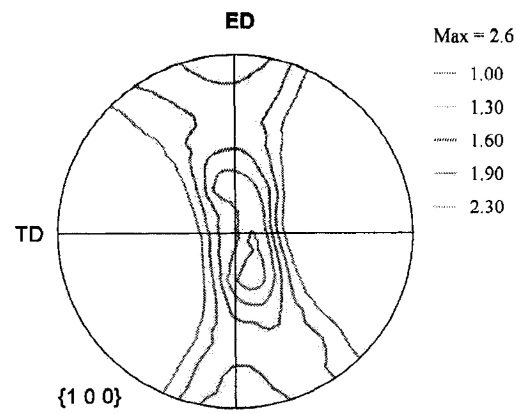

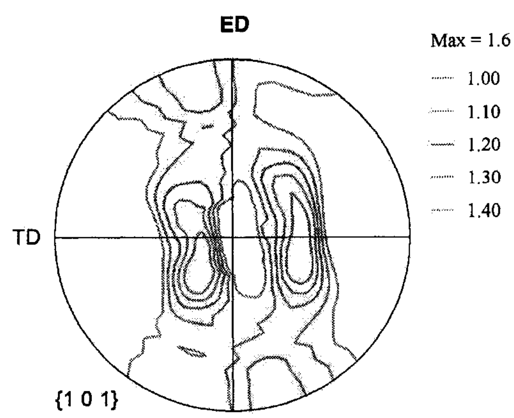

Inverse Pole Figures

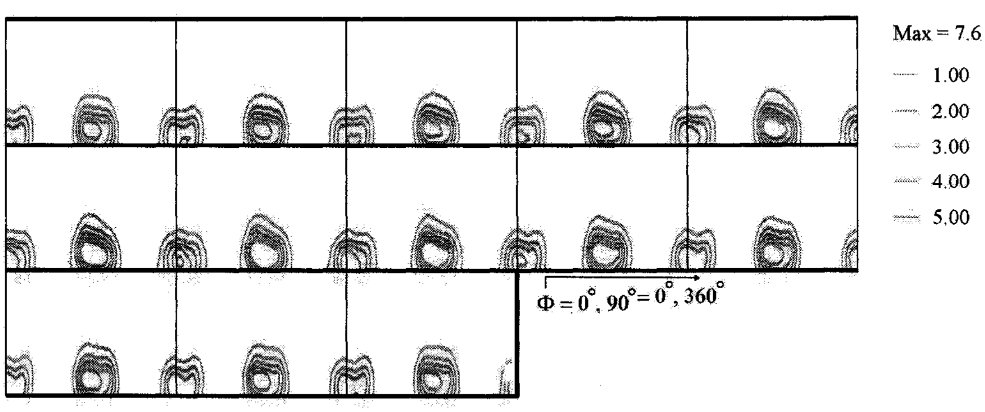

APPENDIX B (cont'd)

Sample Information

Route: A (0° rotation)
Total number of pass(es): 4
Temperature of ECAP: 250°C

Pole Figures

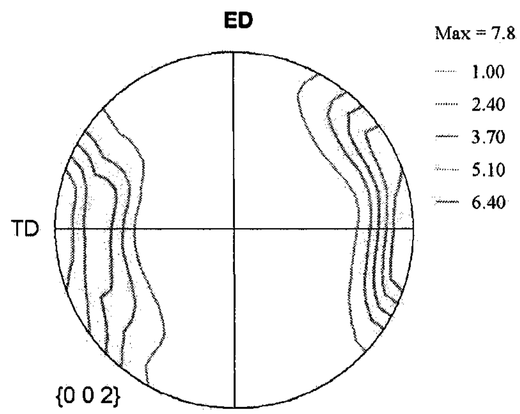

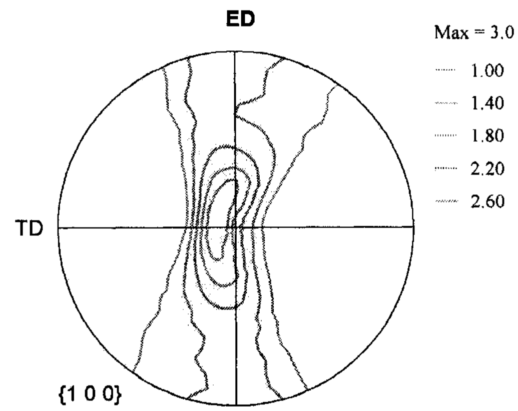

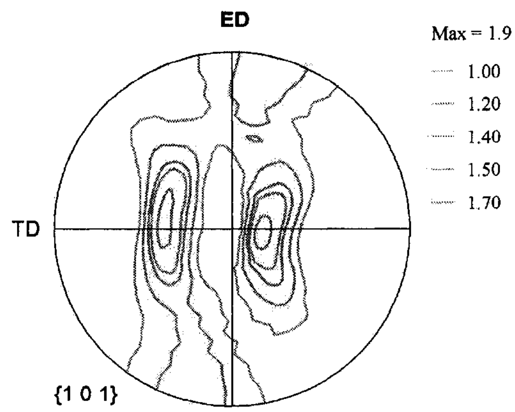

Inverse Pole Figures

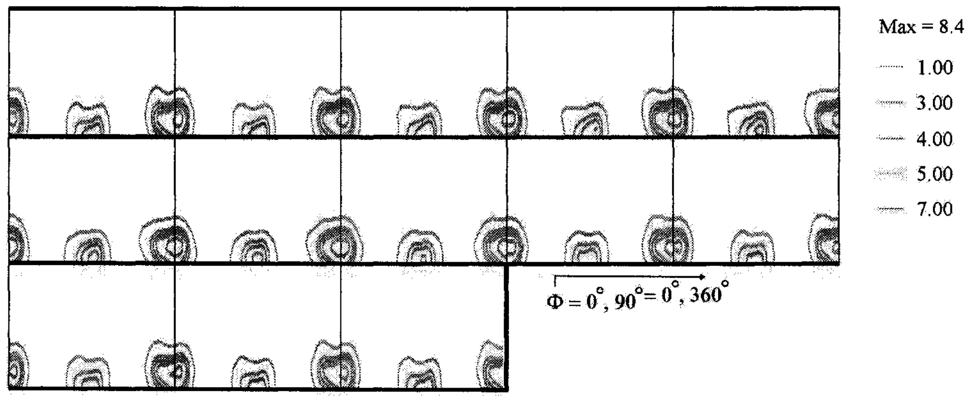

Sample Information

Route: A (0° rotation)
Total number of pass(es): 8
Temperature of ECAP: 250°C

Pole Figures

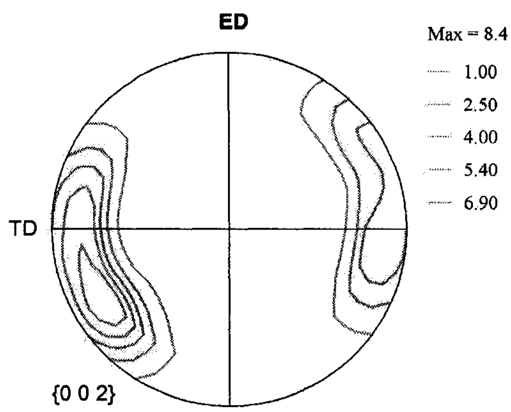

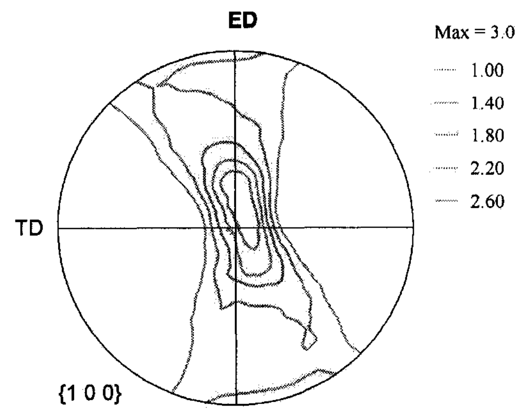

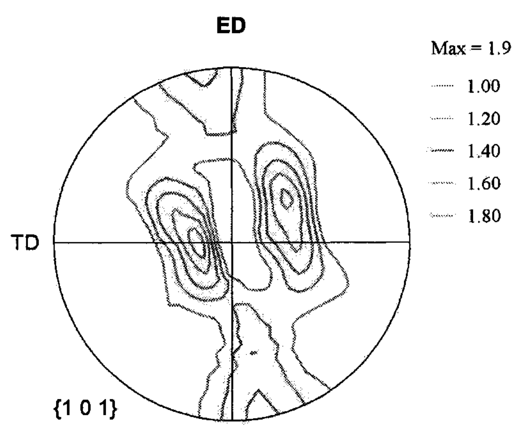

Inverse Pole Figures

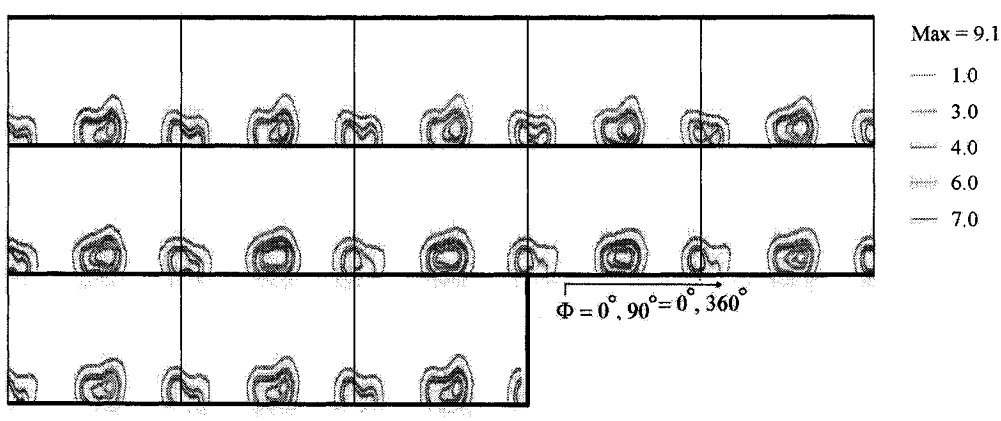

APPENDIX B (cont'd)

Sample Information

Route: C (180° rotation after each pass)
Total number of pass(es): 2
Temperature of ECAP: 250°C

Pole Figures

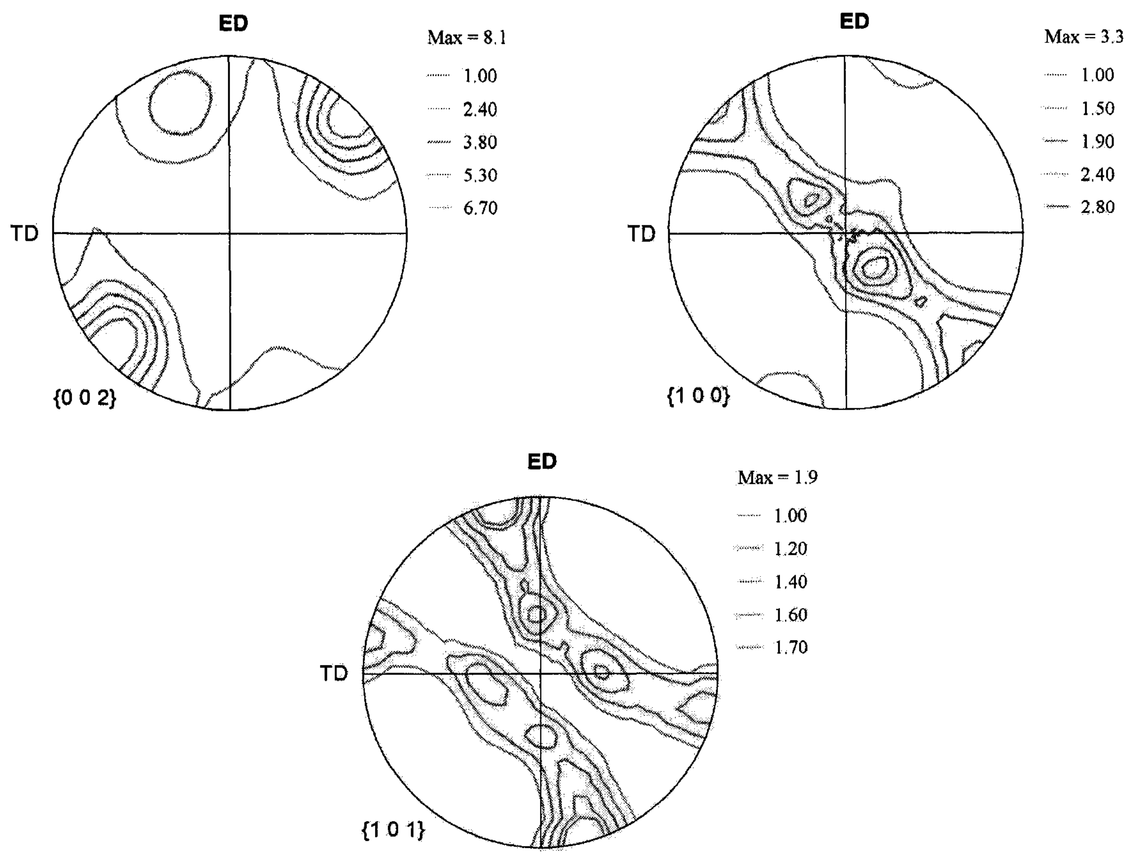

Inverse Pole Figures

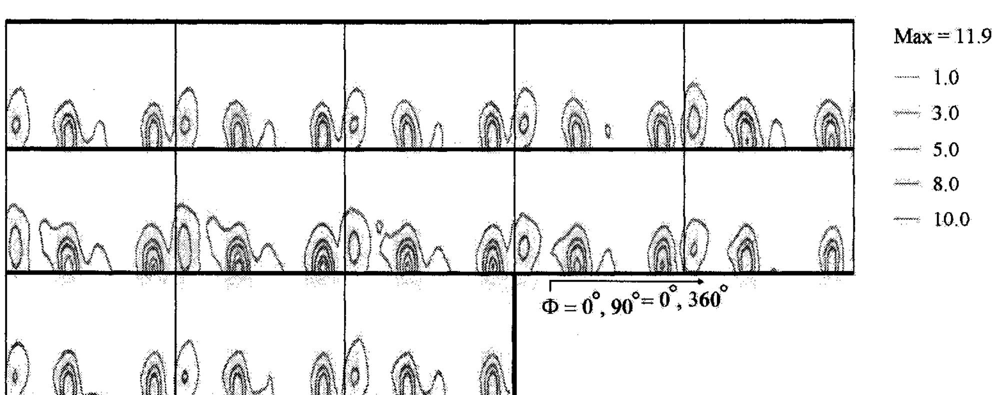

Sample Information

Route: C (180° rotation after each pass)
Total number of pass(es): 4
Temperature of ECAP: 250°C

Pole Figures

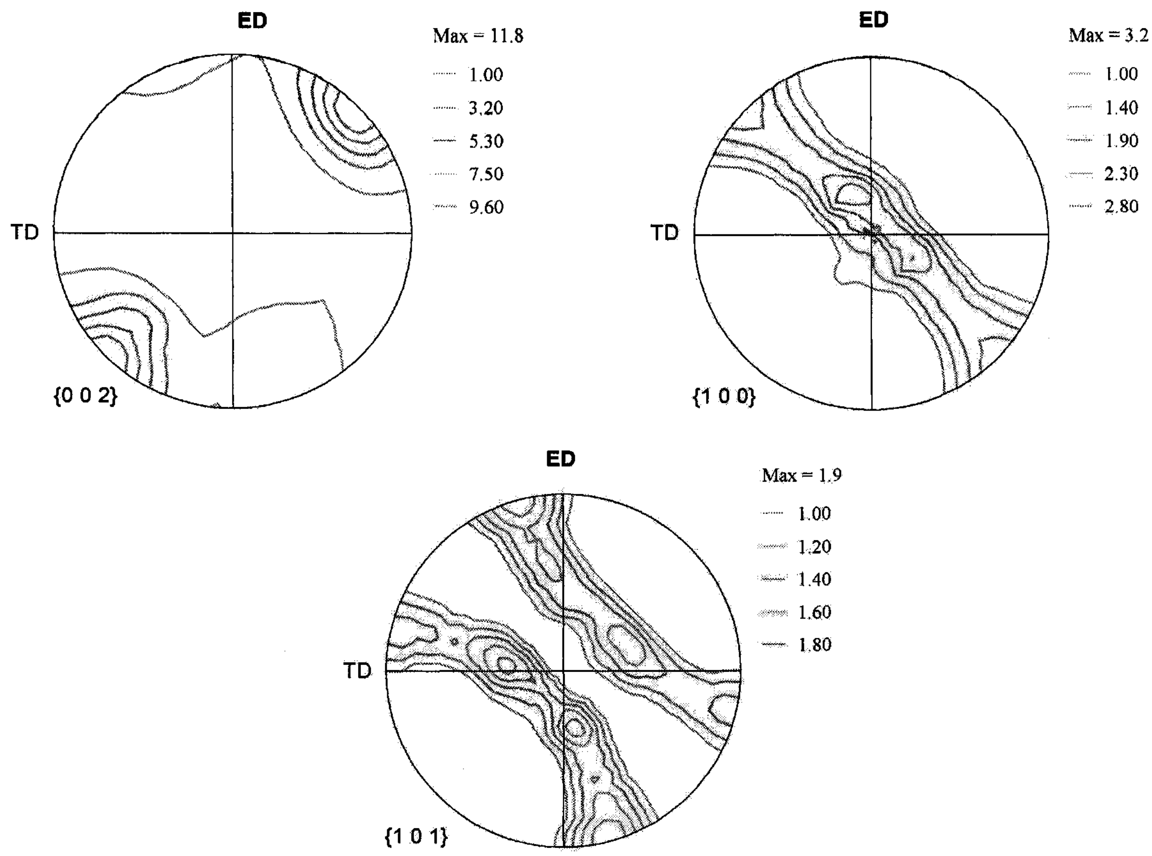

Inverse Pole Figures

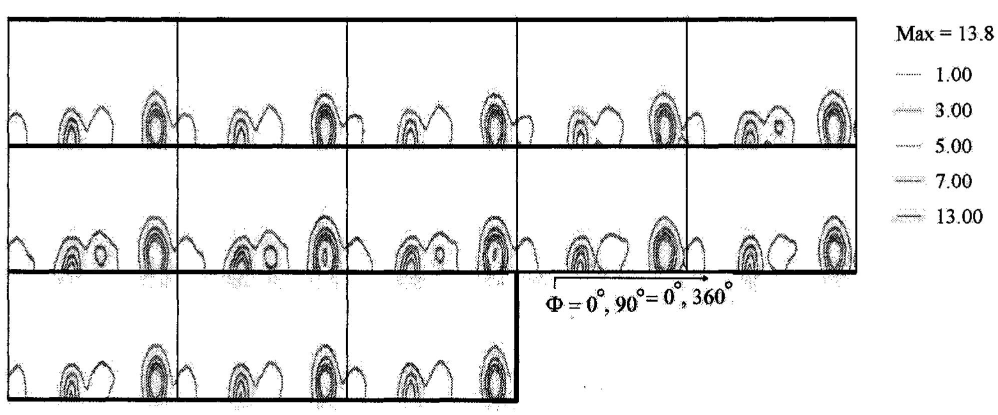

APPENDIX B (cont'd)

Sample Information

Route: C (180° rotation after each pass)
Total number of pass(es): 8
Temperature of ECAP: 250°C

Pole Figures

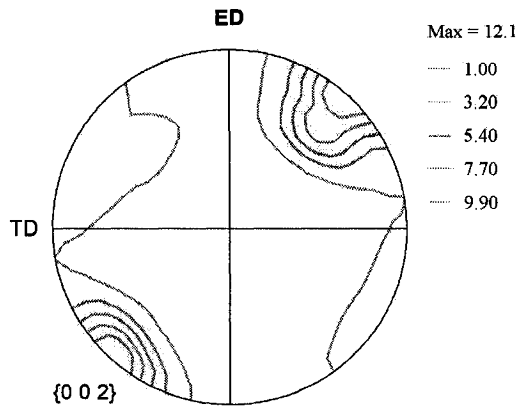

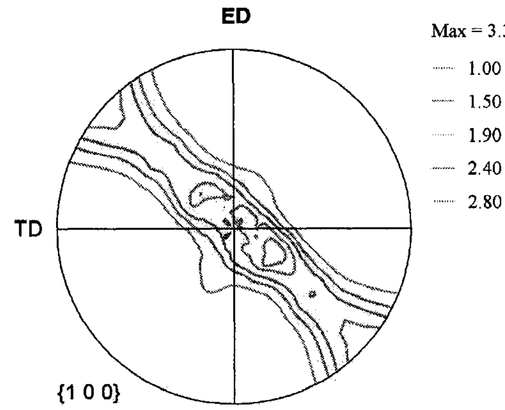

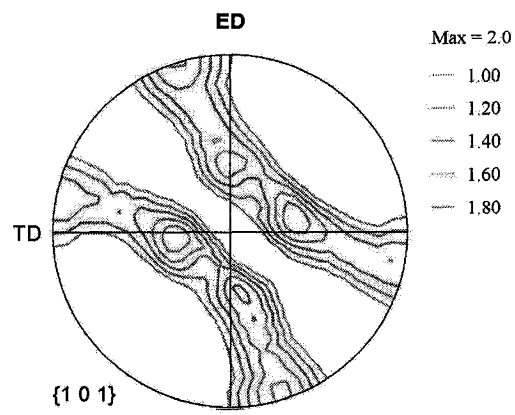

Inverse Pole Figures

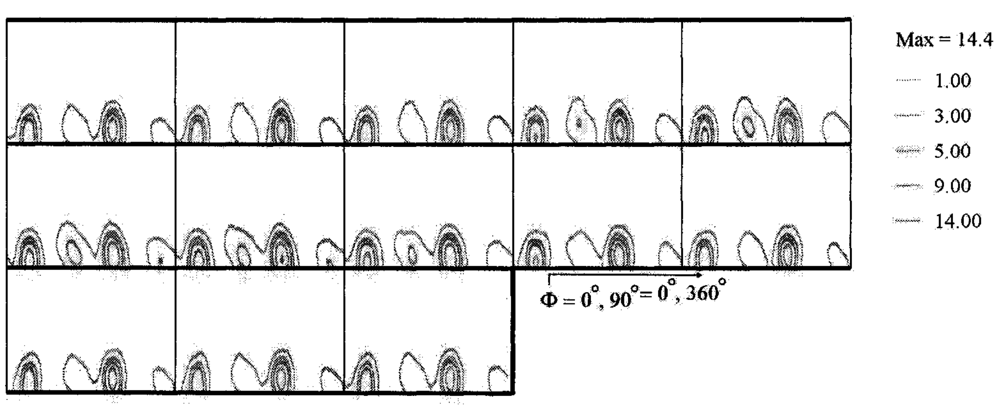

APPENDIX B (cont'd)

Sample Information

Total number of pass(es): 1
Temperature of ECAP: 300°C

Pole Figures

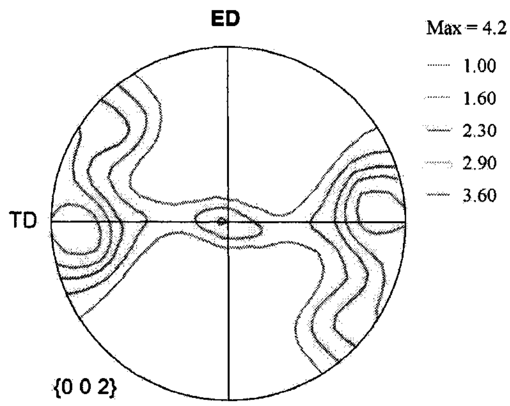

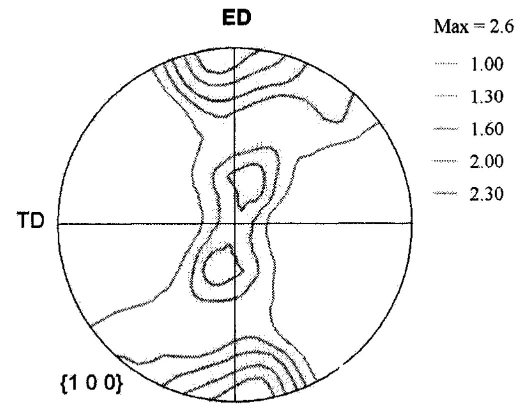

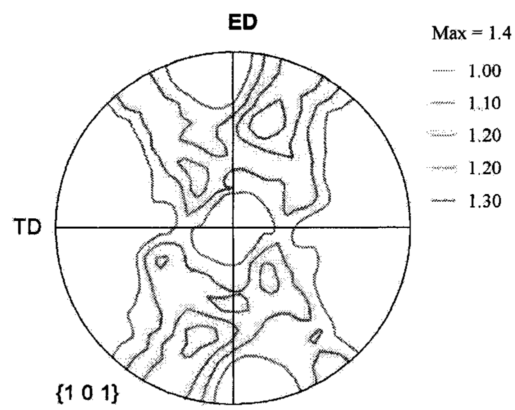

Inverse Pole Figures